

A 98% spectroscopically complete sample of the most powerful equatorial radio sources at 408 MHz

P. N. Best,¹* H. J. A. Röttgering¹ and M. D. Lehnert²

¹ Sterrewacht Leiden, Postbus 9513, 2300 RA Leiden, the Netherlands

² Max-Planck-Institut für extraterrestrische Physik, P.O.Box 1603, 87450 Garching, Germany

1 September 2018

ABSTRACT

A new sample of very powerful radio galaxies is defined from the Molonglo Reference Catalogue, according to the criteria $S_{408\text{MHz}} > 5 \text{ Jy}$, $-30^\circ \leq \delta \leq 10^\circ$ and $|b| \geq 10^\circ$. The sample is selected to have similar properties to the northern 3CR revised sample, and to be visible to a combination of existing northern telescopes such as the Very Large Array radio interferometer and large southern hemisphere telescope facilities. The sample contains 178 sources, of which spectroscopic redshifts are available in the literature for 128. For the remaining 50 sources, new radio imaging, optical imaging and spectroscopic observations are presented to identify the host galaxies and determine their redshifts. With these new observations the total sample is 100% optically identified and redshifts are available for 174 (98%) of the sources. The sample consists of one starburst galaxy, one Seyfert galaxy, 127 radio galaxies and 49 quasars. Basic properties of the sample, such as the distributions of the quasar and radio galaxy populations in redshift and their locations on the radio power versus linear size ($P - D$) diagram, show no significant differences from the revised 3CR sample. The equatorial location and the high spectroscopic completeness of this sample make it a valuable resource for detailed studies of the nature and environments of these important objects with the new generation of southern hemisphere telescopes.

Key words: Galaxies: active — Radio continuum: galaxies — Galaxies: distances and redshifts — Catalogues — Quasars: emission lines

1 INTRODUCTION

Radio sources are unique cosmological probes, with importance for understanding the physics of active galactic nuclei, for studying the relationship between the radio source and its surrounding environment, for probing high redshift proto-cluster environments, and for defining complete samples of galaxies for studies of stellar populations at early epochs. The revised 3CR sample (Laing, Riley & Longair 1983; hereafter LRL) contains the brightest extragalactic radio sources in the northern sky selected at 178 MHz; the host galaxies of these radio sources are predominantly giant elliptical galaxies and lie at redshifts out to $z \sim 2$. Scientifically, the revised 3CR sample has proven exceedingly powerful since it is 100% spectroscopically complete, avoiding many selection biases inherent in less complete samples, and has become established as the standard sample of bright low frequency selected radio sources. The 3CR galaxies and quasars have been the subject of extensive studies over a

wide range of wavelengths leading to many important discoveries, not least of which were the very tight relationship between the infrared K-magnitudes and the redshifts of the radio galaxies (e.g. Lilly and Longair 1984), the discovery that the optical and ultraviolet emission of the high redshift ($z \gtrsim 0.6$) radio galaxies is elongated and aligned along the direction of the radio axis (McCarthy et al. 1987), and the orientation-based unification schemes of radio galaxies and radio loud quasars (e.g. Barthel 1989).

The new generation of large optical telescopes provides an exciting new opportunity for very detailed studies of these important objects and their environments, as has been proven by the results being produced by the Keck telescope (e.g. Cimatti et al. 1996, Dey et al. 1997, Dickinson 1997). Radio astronomy has, however, historically been concentrated in the northern hemisphere, and there is currently no large, spectroscopically complete sample of low frequency selected radio sources equivalent to the 3CR sample for studies with southern hemisphere telescopes such as the VLT and Gemini South. The current paper aims to rectify this deficiency.

The layout of the paper is as follows. In Section 2 the

* Email: pbest@strw.leidenuniv.nl

selection criteria of the new sample are described. Details of the observations that were carried out to provide optical identifications and spectroscopic redshifts for those sources for which such data could not be found in the literature are provided in Section 3. In Section 4, the results of these observations are provided in the form of radio maps, optical images and spectra of these sources. Tabulated details of the resulting complete sample are compiled in Section 5 and global properties of the sample are investigated. Conclusions are summarised in Section 6. Values for the cosmological parameters of $\Omega = 1$ and $H_0 = 50 \text{ km s}^{-1} \text{ Mpc}^{-1}$ are assumed throughout the paper.

2 SAMPLE DEFINITION

The basis dataset for our sample was the Molonglo Reference Catalogue (MRC; Large et al. 1981), a catalogue of radio sources selected at 408 MHz in the region of sky $-85^\circ < \delta < 18.5^\circ$, $|b| \geq 3^\circ$, and essentially complete down to a flux density limit of 1.0 Jy at that frequency. The low frequency selection criterion of this catalogue, like that of the 3CR sample (178 MHz), selects radio sources primarily on the relatively steep spectrum synchrotron emission of their extended radio lobes, rather than on flat spectrum cores, jets and hotspots, and is therefore less subject to Doppler boosting effects than samples selected at higher radio frequencies.

The sample (hereafter the BRL sample) was drawn from the MRC according to four criteria:

- They must have a flux density $S_{408\text{MHz}} \geq 5 \text{ Jy}$.
- They must lie in the region of sky $-30^\circ \leq \delta \leq +10^\circ$.
- They must lie away from the galactic plane, $|b| \geq 10^\circ$.
- They must be associated with extragalactic hosts.

The first selection criterion is similar to the flux density limit of the revised 3CR sample (LRL), $S_{178\text{MHz}} > 10.9 \text{ Jy}$, for a typical radio source with a radio spectral index $\alpha \sim 0.8$ ($S_\nu \propto \nu^{-\alpha}$). The second criterion was made so that the sample would be visible from both northern radio telescopes such as the VLA and southern hemisphere telescopes such as the new large optical telescopes (VLT, Gemini South) and the proposed Atacama Large Millimetre Array (ALMA). The third criterion rejects most galactic objects and avoids the regions of highest galactic extinction.

The first three selection criteria produced a sample of 183 entries in the Molonglo Reference Catalogue. Of these, 0532–054 (M42, Orion) and 0539–019 were excluded on the basis of being galactic HII regions. 0634–204 and 0634–206 appear as two separate entries in the MRC catalogue, whereas they are in fact two parts of the same giant radio source (Baum et al. 1988); these two entries were therefore merged as 0634–205. Similarly, the entries 1216+061A and 1216+061B are from the same source, hereafter referred to as 1216+061 (e.g. see Formanont 1971). Finally, the single catalogue entry 2126+073 (3C435) is actually composed of two individual radio sources (McCarthy et al. 1989) neither of which on its own is luminous enough to make it into the sample, and so these were excluded. 0255+058 (3C75) is also composed of two distinct sources, although overlapping and inseparable in terms of flux density (Owen et al. 1985), but this entry is maintained within the sample since

at least one of the two sources must be sufficiently luminous that it would have entered the sample on its own. These considerations led to a final BRL sample of 178 sources.

Selected in this way the sample is complementary to many other radio source samples which have been constructed or are under construction. The northern declination limit of $+10^\circ$ corresponds to the southern declination limit of the LRL sample. Bright sources more southerly than the -30° declination limit will be included in a new southern sample being prepared by Hunstead and collaborators. Between these three samples, therefore, almost the entire sky (away from the galactic plane) will be covered. The BRL sample further complements the MRC strip 1 Jansky sample defined by McCarthy and collaborators (e.g. McCarthy et al. 1996); the MRC strip, also composed of southern radio sources from the MRC catalogue, is selected to be about a factor of five lower in radio power than our sample and is currently $\gtrsim 75\%$ spectroscopically complete. Due to its larger sky coverage, the BRL sample provides almost a factor of 5 more radio sources at the highest flux densities than the MRC strip, which is essential to provide large enough numbers of the rare high power objects for studies of, for example, the alignment effect or their clustering environments at high redshifts. Combining the BRL sample and the MRC strip will allow variations with radio power to be investigated. Finally, the new sample provides a complement to samples selected at high radio frequencies, such as that of Wall and Peacock (1985), which contain far larger fractions of flat spectrum sources and quasars than low frequency selected samples, due to Doppler boosting effects. The Wall and Peacock sample covers the whole sky away from the galactic plane ($|b| \geq 10^\circ$), contains 233 sources brighter than 2 Jy at 2.7 GHz, and in the region of sky $\delta < +10^\circ$ is over 90% spectroscopically complete (e.g. di Serego Alighieri et al. 1994).

3 OBSERVATIONS AND DATA REDUCTION

A literature search showed that spectroscopic redshifts were already available for 128 of the 178 sources in the sample. Our observations concentrated upon the remaining 50 sources, with the goal of producing a spectroscopically complete sample.

3.1 Radio Imaging

The angular resolution of the observations comprising the Molonglo Reference Catalogue is only about 160 arcseconds in right ascension and in declination varies from about 170 arcseconds at $\delta = -30^\circ$ to 240 arcseconds at $\delta = +10^\circ$. In general these positional uncertainties are too great to allow unambiguous identification of the host radio galaxy or quasar; higher resolution radio data are essential.

Radio data with angular resolution of about 10 arcseconds or less were extracted from the VLA archive for 27 of the 50 radio sources without spectroscopic redshifts. Details of the array configurations and frequencies of these archive data are provided in Table 1. For the remaining 23 sources new observations were made using the VLA during filler time in September 1997 and June 1998 (see Table 1). These observations were single snapshot exposures of typically 5-minute

duration. Either 3C286 or 3C48 was observed during each run for primary flux calibration, and accurate phase calibration was achieved by observations of secondary calibrators within 10–15 degrees of the radio galaxies.

Both the new data and that extracted from the archive were calibrated, CLEANed, and further self-calibrated within the AIPS package provided by the National Radio Astronomy Observatory following standard reduction procedures. The resultant radio maps are shown in Figures 1 to 50.

3.2 3.6m EFOSC2 observations

The optical imaging and spectroscopic observations were carried out predominantly during two observing runs at the ESO 3.6m telescope, La Silla, on 21–22 April 1998 and 20–21 November 1998. The EFOSC2 instrument was used together with the 2048 by 2048 Loral CCD #40 which, after binning 2 by 2 pixels on read-out, provided a spatial scale of 0.315 arcsec per binned pixel. The spectroscopic observations were taken through a 2 arcsecond slit using the grism #6 which provided a wavelength coverage from 3860 to 8070 Å, a scale of 4.1 Å per binned pixel and a spectral resolution of about 22 Å.

The observing technique used was to make first a short image of the field of the radio source through the *R*-Bessel filter and use the VLA radio map to identify the host galaxy or quasar. The telescope was then moved to centre this object in the slit and a spectrum taken. The spectral slit position angle was left in the default east–west direction unless there was good reason to do otherwise, for example if there were two candidate host objects in which case they were both placed along the slit. The duration of the spectral exposure was of between 5 and 20 minutes, depending roughly upon the magnitude of the host object in the *R*-band observation. A second exposure was then begun whilst the first was being reduced. If emission lines were easily visible in the first spectrum then the second exposure was cut short or aborted. Details of the observations are given in Table 1.

Both the imaging and spectroscopic data were reduced using standard packages within the IRAF NOAO reduction software. For the imaging observations the bias level and dark current were first subtracted and then the images were flat-fielded using a flat-field constructed from all of the imaging observations. Photometry was achieved using regular observations of photometric standards throughout the nights.

The raw spectroscopic data frames were bias subtracted, and then flat-fielded using observations of internal calibration lamps taken with the same instrumental set-up as the object exposures. The sky background was removed, taking care not to include extended line emission in the sky bands, and then the different exposures of each galaxy were combined, where appropriate, and cosmic ray events removed. One dimensional spectra were extracted and were wavelength calibrated using observations of CuNe and CuAr arc lamps. Flux calibration was achieved using observations of the spectrophotometric standard stars GD108, G60-54 and LDS749B for the April run, and Feige-24 and L745-46A in November, and the determined fluxes were corrected for airmass extinction.

3.3 WHT observations

Observations of 7 of the sources were made using LDSS2 on the William Herschel Telescope as a backup programme during the first half of the night of 13 August 1998. LDSS2 was used together with a SITe1 2048 by 2048 CCD, providing 0.594 arcseconds per pixel. Imaging observations were made using the broadband Harris-R filter. Spectroscopic observations were taken using the standard long slit with a projected size of 1.4 by 225 arcseconds, and the ‘medium-blue’ grism, providing a scale of 5.3 Å per pixel and a spectral resolution of about 13 Å.

Spectroscopic observations of the sources 1643–223 and 1920–077 were made using the dual-beam ISIS spectrograph on the William Herschel Telescope during morning twilights of 20 and 21 March 1999 respectively. In the blue arm of the spectrograph the R158B grating was used together with a 2096 by 4200 EEV CCD, providing a spectral coverage from the atmospheric cutoff through to longward of the dichroic at 5400 Å, and a spectral resolution of 11 Å. In the red arm the R316R grating was used together with a 1024 by 1024 Tek CCD, providing a spectral resolution of about 5 Å and a spectral range of 1525 Å. This range was centred on 7919 Å for 1643–223 and 8245 Å for 1920–077.

Details of the observations are given in Table 1. The procedures for both the observations and the reduction of the LDSS2 data and the ISIS data mirrored those described for the EFOSC2 observations, except that the default spectral slit orientation for the LDSS data was north–south. Kopff 27 was used for spectrophotometric calibration of the LDSS data, and g193–74 for the ISIS data.

4 RESULTS OF OBSERVATIONS

The host galaxy or quasar of the sources without pre-existing spectroscopic redshifts has been identified from the *R*-band images in all 50 cases. Finding charts for these identifications can be found in Figures 1 to 50; these show a region of 2 by 2 arcminutes, centred upon the host galaxy or quasar. The host objects are indicated by the crosses on the finding charts. Where there may be some ambiguity as to the host object, with more than one object lying within the radio source structure, the justification for the labelled host is given in Section 4.3 on a source by source basis. A magnified view of the central regions can also be found overlaid upon the radio maps in Figures 1 to 50, except for the largest radio sources where this would simply repeat the finding chart view.

The absolute positioning of the optical frames was determined using the positions of between 8 and 12 unsaturated stars on the optical frames that were also present in the APM data base (Maddox et al. 1990) or the Digitized Sky Survey. The optical frames were registered with the sky surveys taking account of possible rotation of the field of view, and then the precise optical position of the host galaxy or quasar was determined. These positions can be found in the sample collation, Table 3. There will remain small astrometric errors between the radio and optical images, due to uncertainties in the absolute alignment of the radio and optical frames of reference. The magnitude of these errors can be judged from the mean positional difference between the

Table 1. Details of the radio, optical imaging and spectroscopic observations.

Source	Radio			Optical Imaging				Spectroscopy			Notes ^a	
	Obs. Date	Array	Freq. [GHz]	Run ^b	Exp. Time [s]	<i>R</i> -magnitude	ID	Slit PA [deg]	Exp. Time [s]	<i>z</i>	δz	
0016-129	19/06/98	BnA	5	3	180	22.81	22.68	RG	0	1500	1.589	0.001
0056-172	Archive	BnA	1.4	3	60	21.11	—	RG	315	900	1.019	0.002
0101-128	19/06/98	BnA	5	3	60	20.05	—	RG	0	420	0.387	0.001
0125-143	19/06/98	BnA	5	3	60	19.14	18.67	RG	270	800	0.372	0.001
0128-264	Archive	A	1.4	3	180	22.58	22.19	RG	270	1350	2.348	0.003
0132+079	Archive	A	5	3	60	20.16	19.79	RG	0	600	0.499	0.001
0219+082	19/06/98	BnA	5	3	60	18.63	17.98	RG	270	300	0.266	0.001
0310-150	Archive	B	1.4	3	240	21.74	21.71	RG	270	1140	1.769	0.003
0357-163	19/06/98	BnA	5	3	180	20.56	20.40	RG	270	900	0.584	0.002
0406-180	Archive	BnA	1.4	3	120	19.21	19.12	Q	270	900	0.722	0.001
0519-208	Archive	BnA	5	3	240	21.91	21.80	RG	270	840	1.086	0.002
0850-206	Archive	B	1.4	1	300	22.07	21.93	RG	270	2400	1.337	0.002
0851-142	17/09/97	C	8	1	300	22.63	22.41	RG	270	2400	1.665	0.002
1039+029	Archive	A	5	1	300	21.27	20.96	RG	270	1800	0.535	0.002
1059-010	17/09/97	C	8	1/3	300	24.20	—	RG	270	1800	—	—
1131-171	17/09/97	C	8	1	300	19.01	19.01	Q	270	1200	1.618	0.002
1138+015	Archive	A	5	1	300	20.03	19.48	RG	270	900	0.443	0.002
1140-114	Archive	A	1.4	1	300	23.01	22.95	RG	270	2400	1.935	0.001
1303+091	Archive	A	5	1	300	22.12	22.16	RG	270	2400	1.409	0.002
1307+000	Archive	C	5	1	300	19.56	—	RG	270	900	0.419	0.001
1344-078	Archive	B	1.4	1	300	19.73	19.30	RG	270	900	0.384	0.002
1354+013	Archive	A	5	1	300	21.79	21.44	RG	270	1200	0.819	0.001
1411-057	17/09/97	C	8	1	300	22.39	22.23	RG	270	2400	1.094	0.002
1413-215	29/06/98	BnA	5	1	300	22.67	—	RG	—	—	—	N
1422-297	Archive	B	1.4	1	300	22.55	22.50	RG	270	1650	1.632	0.001
1434+036	Archive	A	5	1	300	21.49	21.53	Q	270	1650	1.438	0.001
1436-167	Archive	B	1.4	1	30	17.31	16.26	RG	270	240	0.146	0.001
1509+015	Archive	A	5	1	300	21.61	21.25	RG	270	900	0.792	0.002
1602-093	Archive	C	5	1	180	18.01	16.97	RG	270	1200	0.109	0.001
1602-174	29/06/98	BnA	5	1/2	300	21.69	21.40	RG	270	960	2.043	0.002
1602-288	29/06/98	BnA	5	1/2	300	20.43	19.82	RG	240	1300	0.482	0.001
1603+001	Archive	A	5	1	30	16.47	14.98	RG	270	120	0.059	0.001
1621-115	Archive	C	1.4	1	300	19.79	—	RG	270	2100	0.375	0.002
1628-268	29/06/98	BnA	5	2	180	19.10	17.92	RG	0	1500	0.166	0.003
1643+022	Archive	A	5	1	60	17.02	—	RG	270	300	0.095	0.001
1643-223	29/06/98	BnA	5	1/4	240	19.25	—	Q	270	900	0.799	0.003
1649-062	Archive	C	1.4	1	300	19.05	18.41	RG	270	300	0.236	0.002
1716+006	Archive	A	5	1	300	19.98	19.89	Q	270	1200	0.704	0.001
1732-092	29/06/98	BnA	5	2	60	19.43	19.41	RG	0	900	0.317	0.001
1810+046	Archive	A	5	1	300	19.08	19.06	Q	270	1200	1.083	0.002
1859-235	28/06/98	BnA	5	2	300	20.82	—	RG	0	1200	—	N
1912-269	28/06/98	BnA	5	2	300	18.62	17.49	RG	0	960	0.226	0.001
1920-077	28/06/98	BnA	5	2/4	300	21.51	—	RG	20	1200	0.648	0.001
1953-077	28/06/98	BnA	5	2/3	420	22.90	—	RG	340	1200	—	N
2025-155	28/06/98	BnA	5	3	120	19.86	—	Q	300	1700	1.500	0.003
2120-166	28/06/98	BnA	5	3	120	20.93	20.94	RG	270	820	0.882	0.001
2128-208	28/06/98	BnA	5	3	90	19.49	19.46	Q	270	960	1.615	0.004
2318-166	Archive	BnA	1.4	3	180	21.47	21.45	RG	270	900	1.414	0.001
2322-052	28/06/98	BnA	5	3	360	22.98	22.38	RG	270	3300	1.188	0.002
2347-026	Archive	A	1.4	3	180	22.95	22.74	RG	270	900	1.036	0.001

^a Notes can be found in Section 4.3 for sources marked with an N.^b Where two run numbers are given the first is for imaging, the second for spectroscopy. The run numbers correspond to:

1 — EFOSC2 at the ESO 3.6m, April 21–22 1998.

2 — LDSS2 at the WHT, August 13 1998.

3 — EFOSC2 at the ESO 3.6m, November 20–21 1998.

4 — ISIS at the WHT, March 20–21 1999.

^c For $\Omega = 1$ and $H_0 = 50 \text{ km s}^{-1} \text{ Mpc}^{-1}$

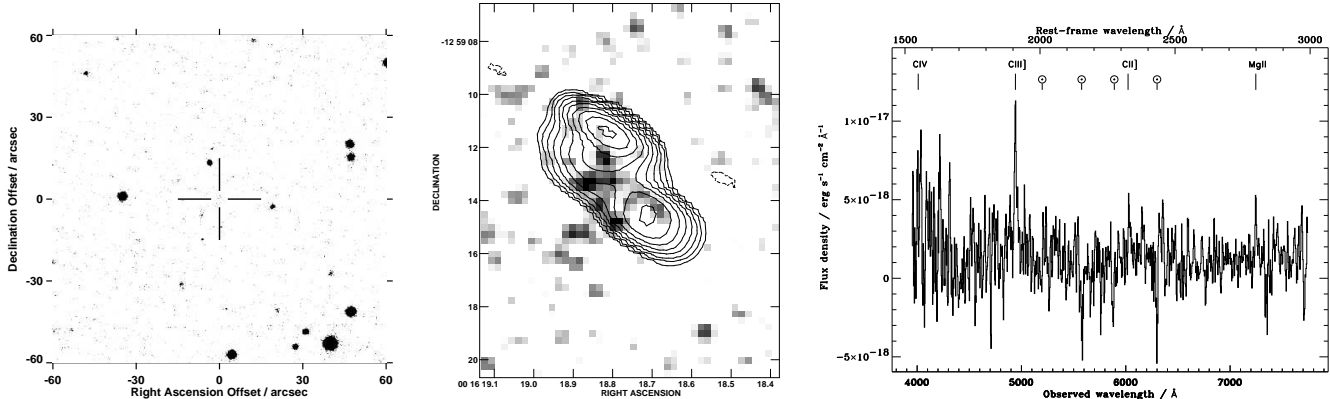


Figure 1. (a) an R -band finding chart of size 120 by 120 arcseconds for 0016–129; (b) a zoomed view of the host galaxy, with contours of the radio emission overlaid (the contour levels are increasing by factors of 2 from the first contour at 0.5 mJy/beam); (c) the spectroscopic data with the identified emission and/or absorption lines labelled. Sky features are indicated by an open circle with a central dot

VERSION INCLUDING FIGURES 2 TO 50 AVAILABLE FROM <http://www.strw.leidenuniv.nl/~pbest/equatpap.ps>

optical centre of a radio galaxy or quasar and the position of a radio core, where the latter is detected. Unambiguous radio cores or unresolved radio sources (from a high resolution map) are observed for 21 of the sources presented here; there is no systematic offset between the radio core and the optical centre, and the root-mean-squared separation is 0.55 arcseconds. This therefore is the accuracy to which the radio and optical frames can be overlaid. Note that where there is an offset between the radio core position and the position of the optical identification in our data, it is the position of the optical source which is given in Table 3.

For 46 of the 50 galaxies a spectroscopic redshift was obtained. The spectra are shown in Figures 1–50 with the identified lines labelled, the resulting redshift being given in Table 1. The uncertainties of the peak positions of the measured emission lines and the variation in the measured redshift between different lines in the spectrum were both determined, and the larger of these values (generally the latter) was adopted as the uncertainty on the galaxy redshift. In four cases (1039+029, 1509+015, 1649–062, 2322–052) the redshift was based upon only weak emission lines, or a single strong emission line together with some weak confirming feature; notes on these sources are provided in Section 4.3. For the four sources for which no spectroscopic redshift has been obtained (1059–010, 1413–215, 1859–235, 1953–077), a discussion is also provided in Section 4.3.

4.1 Emission line properties

Various properties of the emission lines have been determined and are provided in Table 2. The flux of each emission line was determined by summing the intensities of the pixels above a fitted continuum level over a wavelength range of four times the fitted (pre-deconvolution) full-width at half-maximum (FWHM) of the line. The uncertainty in the measured flux of each emission line was calculated taking account both of the measurement error from the limited

signal-to-noise of the emission line, and an uncertainty in the flux calibration, assumed to be 10%. Note that caution must be applied to the use of the derived emission line fluxes, since they are measured only from the portion of the galaxy sampled by the slit and therefore, especially at low redshifts, are lower than the total line flux emitted by the galaxy. These line fluxes should not be used to investigate the variation of emission line strengths as a function of redshift. The ratios of the line fluxes for lines not widely separated in wavelength should provide an accurate measure, although for widely separated lines caution should again be adopted since atmospheric diffraction means that the red and blue ends of the spectrum might be sampling different regions of the galaxy.

Also calculated are the deconvolved FWHM of the emission lines, determined assuming that the lines follow a Gaussian profile. The uncertainty in this deconvolved width is a combination of the uncertainty in the measured FWHM due to the limited signal-to-noise ratio of the line, and deconvolution errors introduced by the uncertainty in the spectral resolution of the observations, estimated to be 10%. Where the fitted FWHM was found to be less than the resolution, or the deconvolved FWHM was determined to be less than its error, the uncertainty in the deconvolved FWHM has been adopted as an upper limit to the deconvolved FWHM. Due to the low spectral resolution of these observations, this was frequently the case, and little velocity information was obtained except for the broadest lines. Finally, the equivalent widths of the emission lines were calculated, along with their errors. Where the equivalent width was determined to be smaller than 1.5 times its error, a value of twice the error in the equivalent width has been adopted as an upper limit to the line equivalent width.

4.2 Optical magnitudes and classifications

R-band magnitudes were measured for the host galaxy or quasar, after any faint objects close to the radio source host but not obviously a part of it had been edited out of the image. The local sky level was determined within a concentric annulus centred upon the host object with an inner radius of between 5 and 10 arcseconds, chosen to avoid contamination from nearby objects, and a width of 2 or 3 arcseconds. Where it was impossible to avoid faint objects within the sky annulus, these objects were edited out of the image before photometry was performed. In 5 cases (1307+000, 1643–223, 1859–235, 1912–269, 1920–077) it was impossible to avoid nearby bright objects, or large numbers of faint objects, falling within the sky annulus. In these cases the local sky level was estimated using regions of empty sky close to the host galaxy or quasar at a range of different position angles.

The *R*-band magnitude was determined through two different aperture sizes. First, a 4 arcsecond diameter aperture was used, chosen to allow comparison with the measurements of McCarthy et al. (1996) for the Molonglo strip sources. Such a measurement was possible for all of the objects, since none had significant contributions from other objects at these radii. It should be noted, however, that this aperture measurement seriously underestimates the luminosity of low redshift galaxies (for quasars there is little dependence of the *R*-magnitude upon aperture diameter). The second aperture adopted was a fixed metric aperture of 63.9 kpc diameter; such an aperture is large enough to contain essentially all of the light from the galaxies, the specific value of 63.9 kpc being chosen for comparison with the measurements of Eales et al. (1997). Determination of the *R*-magnitude through a 63.9 kpc aperture was not possible in all cases: for the 4 sources without redshifts, the aperture diameter corresponding to 63.9 kpc is unknown; for 8 other sources, nearby objects too bright to be accurately edited out of the image prevented measurement of the flux out to these radii.

The *R*-band magnitudes of the host galaxies and quasars through these two apertures are provided in Table 1. Notice the large differences, up to 1.5 magnitudes, between the two values for the low redshift galaxies. The uncertainties on the measurements of these magnitudes are about 0.1 magnitudes for $R \lesssim 21$, increasing to about 0.3 magnitudes by $R \approx 23$.

The nature of optical identification was classified based upon optical appearance of the image and the presence of broad emission lines, that is, emission lines with a deconvolved FWHM greater than 2000 km s^{-1} , with an uncertainty sufficiently low that the FWHM minus its uncertainty is above 1500 km s^{-1} . If the optical image contained an unresolved component of absolute luminosity[†] $M_R < -24$ (roughly equivalent to the $M_B < -23$ limit in the quasar catalogue of Véron-Cetty & Véron 1996; cf. the discussion in Willott et al. 1998), and broad emission lines, then the object was classified as a quasar. This was true for eight

[†] To calculate the K-correction needed to derive absolute magnitudes, a power-law slope of spectral index 0.7 was assumed for the point source continuum.

of the fifty cases. Of the remainder, 0850–206, 1140–114, 1436–167 are all well-resolved and show narrow forbidden lines, but their permitted lines are broad. These sources were therefore classified as broad-line radio galaxies. 1732–092 also shows broad permitted lines, and some of its emission comes from an unresolved component, but that component is not sufficiently luminous to be classified as a quasar and so it also is classified as a broad-line radio galaxy. The remainder of the identifications are well resolved with only narrow lines and so are classified as radio galaxies.

In Figure 51 the *R* magnitudes are plotted against the redshift of the source, showing the radio galaxies and quasars separately. The $R - z$ diagram for the radio galaxies shows the well-known tight correlation out to about a redshift of 0.8 (e.g. Eales 1985), beyond which the scatter increases due to different strengths of the alignment effect in different sources. This diagram is powerful because the $R - z$ correlation can be used to provide supporting evidence for redshifts determined from only weak features, and to estimate the redshifts of the 4 remaining sources from their *R*-magnitudes. The quasars have brighter *R*-magnitudes than would be expected from the $R - z$ relation of the radio galaxies, due to their AGN component.

4.3 Notes on individual sources

0056–172: The optical identification of this source is the south-westerly of the two objects lying along the radio source axis; the north-eastern object shows no strong emission lines.

0125–143: The optical identification, showing powerful line emission, is the brighter of the two objects and is coincident with the radio core.

0128–264: The identification is the faint aligned object lying directly along the radio axis. The high background level in the south-west is caused by a nearby bright star.

0357–163: The host galaxy appears to lie coincident with the eastern hotspot (possibly the core if a faint radio lobe has been missed), but this identification is secure: the galaxy shows strong emission lines and no other object is observed within the radio source structure.

0850–206: The host radio galaxy, showing powerful emission lines, is the more southerly of the two objects within the radio source structure.

1039+029: The redshift of this source is based upon a single strong emission line which, owing to its high flux, is assumed to be [OII] 3727. This assumption is supported by the detection of a spectral break, consistent with being at 4000 \AA rest-frame, and by the consistency of the *R*-magnitude of this galaxy with the $R - z$ relationship if it is at that redshift (see Figure 51).

1059–010: No spectroscopic redshift has been obtained for this source; the only spectroscopic observations have been carried out during twilight conditions. The proposed host galaxy is extremely faint ($R > 24$), detected at only the $\sim 4\sigma$ level, but is the only possible identification found. The location of this galaxy at the centre of the radio source and its elongation along the radio axis (as is common of high redshift radio galaxies) add to its believability. Comparing

the R -magnitude of this galaxy with the $R - z$ relationship suggests a minimum redshift of about 1.5.

1131–171: The northern of the two objects within the radio source structure, a high redshift quasar, is the host identification for this radio source.

1344–078: It is the object 2 arcseconds north of the centre of the radio source (RA 13 44 23.60, Dec –07 48 25.2) which shows strong emission lines and is therefore identified as the radio source host galaxy.

1413–215: No spectroscopic redshift has been obtained for this source. At the time of the imaging and spectroscopic observations, only a low (~ 60 arcsec) resolution NVSS radio map was available and this indicated a radio position 10 arcseconds south of the true core due to the asymmetry between the northern and southern hotspot strengths. Given this, there was no obvious host galaxy identification, and so no spectroscopic observations were attempted. The new high resolution VLA map provides an unambiguous optical identification, whose R -band magnitude suggests that it is above a redshift of one (cf. Figure 51).

1422–297: The optical identification is the brighter of the two objects towards the centre of the radio source. The fainter object shows no strong emission lines.

1434+036: This source is classified as a quasar on account of a sufficiently luminous unresolved optical component. Its broad MgII 2799 emission (FWHM 2460 ± 408 km s $^{-1}$) is relatively low for quasars, and the R -magnitude lies almost within the scatter of the radio galaxy $R - z$ relation at this redshift, and so the quasar component is likely to be not extremely powerful.

1509+015: The redshift for this galaxy is based predominantly upon one very luminous emission line, assumed to be [OII] 3727; only a weak emission line consistent with being MgII 2799 and a potential 4000Å break are seen to support this. Some corroborating evidence is given by the R -magnitude of the galaxy, which is consistent with the $R - z$ relationship of the sample if this redshift is correct.

1602–174: The emission line object identified as the host galaxy of this radio source is the faint galaxy aligned along the radio axis, coincident with the radio core.

1602–288: The two-dimensional spectrum along the radio axis shows emission lines covering an angular extent of over 20 arcseconds (see Figure 31), which at a redshift of 0.48 corresponds to a spatial extent of nearly 150 kpc. This emission line region extends through both of the objects lying directly along the radio axis, centred close to the fainter of the two objects. The continuum shape of this fainter object (RA 16 02 6.65, Dec –28 51 5.2) resembles an intermediate redshift radio galaxy, whilst the brighter object (ignoring the emission lines) is unresolved and spectroscopically a star. Therefore, although the brighter object is coincident with what has the appearance of a radio core, it is the fainter object which is identified as the host radio galaxy.

1621–115: The object at the centre of the radio contours shows emission lines and so is identified as the host radio galaxy.

1649–062: The optical identification lies very close to the centre of this large radio source. The galaxy shows only very weak emission lines; its redshift is based upon a weak

[OII] 3727 emission line and three absorption features. The other object close to the radio source centre is a star.

1716+006: This source is classified as a quasar since, apart from a very close companion, its optical emission is unresolved. The H γ line, although weak, appears broad (FWHM of 3473 ± 626 km s $^{-1}$). The R -band magnitude of this object is about 1.5 magnitudes brighter than the $R - z$ relation of the radio galaxies at that redshift, support the interpretation of a significant quasar component.

1732–092: The optical identification is the object lying coincident with the bright knot of radio emission. This object is mostly unresolved, but the unresolved component does not contain sufficient flux for it to be classified as a quasar. Its R -magnitude is comparable to those of radio galaxies at this redshift. The galaxy shows clearly broad emission lines so is identified as a broad-line radio galaxy.

1859–235: The identification lies towards the centre of the radio source and so is reasonably secure, although no spectroscopic redshift was obtained for this source in a 20 minute spectrum (albeit taken at a mean airmass of 1.9). The R -band magnitude suggest a redshift in the range 0.3 to 0.9 (cf. Figure 51).

1920–077: The object lying in the gap between the two radio lobes is identified as the host galaxy on the grounds of its location, its resolved emission (many of the objects seen in the image are stellar), and the fact that it shows powerful line emission.

1953–077: The object close to the southern radio lobe is a very likely candidate host galaxy, also on the basis of a detection at the same location in a short exposure J-band image made with WHIRCAM, the infrared imager on the WHT. A spectrum of this object taken during twilight conditions failed to yield a redshift for the galaxy, but the faintness of the R -magnitude indicates that the galaxy is above a redshift of one.

2025–155: It is the fainter (north-eastern) of the two objects seen close to the radio source that shows line emission and is identified as the host object. This object is unresolved, shows a power-law type spectrum, and has an R -magnitude about 3 magnitudes brighter than the mean $R - z$ relationship and so is identified as a quasar.

2128–208: The brighter (eastern) of the two sources is identified as a quasar, and is the host of this radio source. The western object shows no strong emission lines.

2322–052: The region of faint diffuse emission close to the eastern radio lobe shows powerful line emission and is identified as the host radio galaxy. Two emission lines are unambiguously detected with wavelengths consistent with being CIII] 2326 and MgII 2799 at a redshift of 1.188. Weak features consistent with [OII] 2470 and [NeV] 3426 provide supporting evidence, although it is surprising that CII] 1909 is not seen. The R -magnitude of the host galaxy is also consistent with the proposed redshift.

5 THE COMPLETE SAMPLE

5.1 Sample Collation

In Table 3, details are collated of all 178 radio sources in the complete BRL sample. The right ascension and declina-

Table 2. Emission line properties of the objects for which spectroscopic observations were made. See text for details.

Source & Line	Flux / 10^{-16} [erg/s/cm 2]	FWHM [km s $^{-1}$]	E.W. [\AA]
---------------	------------------------------------	----------------------	-----------------------

0016-129

CIV	1.6	\pm 0.5	< 2985	31	\pm 14
CIII]	2.6	0.6	< 911	63	35
CII]	1.2	0.4	< 1657	< 64	
MgII	0.6	0.3	< 525	< 32	

0056-172

CIII]	1.4	\pm 0.5	< 559	11	\pm 4
CII]	0.7	0.4	< 1026	5	2
NeIV	2.2	0.4	< 473	17	3
MgII	4.7	0.6	1952	\pm 686	39
[NeV]	1.2	0.2	< 331	11	2
[NeV]	2.5	0.3	< 313	26	4
[OII]	14.6	1.5	803	269	159

0101-128

[OII]	18.2	\pm 2.1	1039	\pm 446	234	\pm 72
H β	1.7	0.4	< 484		8	2
[OIII]	9.2	1.0	702	314	50	6

0125-143

[OII]	16.2	\pm 1.8	983	\pm 438	56	\pm 7
H β	8.6	1.6	< 7770		17	3
[OIII]	6.4	0.9	< 458		14	2
[OIII]	12.4	1.5	832	393	29	3

0128-264

Ly α	7.9	\pm 1.4	1755	\pm 1160	< 292
CIV	1.1	0.1	1636	983	113
CIII]	0.6	0.6	< 2351		< 30

0132+079

MgII	1.3	\pm 0.9	< 2270		< 20
[NeV]	2.4	0.5	< 572		16
[OII]	8.8	0.9	592	371	60
[NeIII]	1.8	0.3	< 409		10
H β	1.7	0.3	< 352		8
[OIII]	12.5	1.3	< 278		63
[OIII]	32.9	3.3	< 264		169

0219+082

[OII]	21.8	\pm 2.6	< 465	76	\pm 12
[NeIII]	2.6	1.1	< 964	7	3
H γ	1.7	1.0	1106	1027	2
H β	2.9	1.2	< 471		3
[OIII]	24.9	2.6	829	332	32

0310-150

CIV	10.2	\pm 1.5	2323	\pm 1348	84	\pm 30
HeII	4.0	0.8	810	794	33	10
CIII]	5.0	0.8	3051	2204	56	13
CII]	2.2	0.5	882	747	43	16

0357-163

MgII	6.1	\pm 1.1	2078	\pm 1493	61	\pm 15
[NeV]	2.2	0.5	< 1511		20	5
[OII]	6.7	0.7	< 346		62	8
[NeIII]	1.9	0.3	< 479		15	3
H β	1.4	0.4	< 441		9	2

0406-180

MgII	15.0	\pm 1.8	7126	2775	22	\pm 2
[NeV]	3.1	0.4	< 401		4	0
[OII]	14.0	1.5	662	319	21	2
[NeIII]	5.4	0.6	< 331		8	1
H δ	2.0	0.7	< 2329		3	1
H γ	8.1	1.1	2601	841	13	1

Table 2. cont. Emission line properties.

Source & Line	Flux / 10^{-16} [erg/s/cm 2]	FWHM [km s $^{-1}$]	E.W. [\AA]
0519-208			
CIII]	6.0	\pm 1.1	1597
CII]	0.9	0.4	< 787
MgII	3.4	0.6	2494
[NeV]	3.2	0.5	707
[OII]	11.7	1.2	795
			275
			274
			81
0850-206			
CIII]	2.1	\pm 0.2	1180
CII]	0.9	0.1	2587
NeIV	1.7	0.2	988
MgII	1.9	0.2	2384
			323
			48
			4
0851-142			
CIV	3.4	\pm 0.4	961
HeII	2.3	0.3	< 536
CIII]	1.6	0.2	< 440
NeIV	0.6	0.1	907
MgII	2.2	0.4	6088
			5895
			< 736
1039+029			
[OII]	1.5	\pm 0.2	< 359
			30
			\pm 3
1131-171			
CIV	186.4	\pm 18.8	7085
HeII	6.8	1.2	< 482
CIII]	39.0	4.0	4813
NeIV	6.7	0.8	8418
			3418
			3
			1
1138+015			
[OII]	30.5	\pm 3.5	1062
H δ	1.9	1.6	< 1684
H γ	0.5	2.7	< 7361
H β	3.6	2.6	< 1959
[OIII]	1.7	0.9	< 9789
[OIII]	3.8	3.1	< 2474
			< 26
1140-114			
CIV	1.0	\pm 0.3	2878
HeII	0.5	0.1	< 450
CIII]	0.6	0.1	< 393
CII]	1.9	0.3	3686
			1069
			65
			16
1303+091			
HeII	2.6	\pm 0.3	< 577
CIII]	3.5	0.4	981
NeIV	1.0	0.1	< 377
MgII	2.7	0.3	1232
			341
			43
			4
1307+000			
[NeV]	1.6	\pm 0.4	< 758
[OII]	18.9	1.9	< 375
[NeIII]	2.8	0.4	< 375
[OIII]	9.0	1.0	< 289
[OIII]	27.9	2.8	< 279
			74
			7
1344-078			
[NeV]	3.1	\pm 0.6	2873
[OII]	11.4	1.2	574
H γ	0.7	0.5	1688
H β	2.2	0.4	< 558
[OIII]	4.7	0.6	< 325
[OIII]	15.5	1.6	< 290
			51
			5
1354+013			
[NeV]	0.6	\pm 0.2	< 792
[OII]	6.4	0.7	425
[NeIII]	0.5	0.2	< 370
			307
			95
			15
			6
			2

Table 2. cont. Emission line properties.

Source & Line	Flux / 10^{-16} [erg/s/cm 2]	FWHM [km s $^{-1}$]	E.W. [Å]
---------------	------------------------------------	----------------------	----------

1411-057

CIII]	1.1	\pm 0.2	< 781	25	\pm 6
MgII	0.5	0.2	1692	\pm 1481	16
[NeV]	0.5	0.2	< 530	15	5
[OII]	3.2	0.4	< 266	118	27

1422-297

CIV	4.3	\pm 0.6	1662	\pm 954	61	\pm 16
HeII	2.1	0.4	1943	1838	30	8
CIII]	1.0	0.2	< 504	19	4	
NeIV	0.6	0.1	532	484	13	3

1434+036

HeII	5.5	\pm 0.6	675	\pm 567	44	\pm 7
CIII]	2.7	0.3	< 491	24	3	
NeIV	0.8	0.1	< 339	10	1	
MgII	0.8	0.2	2460	408	11	3

1436-167

[NeV]	4.9	\pm 1.0	< 508	6	\pm 1
[OII]	124.7	12.6	775	468	140
[NeIII]	15.2	2.1	< 500	14	2
H γ	2.1	1.8	1467	787	< 6
H β	22.8	2.4	< 358	10	1
[OIII]	144.7	14.5	< 349	68	6
[OIII]	344.2	34.4	580	345	162
[OI]	19.5	2.2	< 464	9	1
H α	332.3	33.3	2180	267	178
[SII]	105.0	10.6	843	268	57

1509+015

MgII	1.2	\pm 0.3	1426	\pm 1341	47	\pm 19
[OII]	5.6	0.6	656	307	108	15

1602-093

[OII]	5.8	\pm 7.9	< 3577	< 40		
-------	-----	-----------	--------	------	--	--

1602-174

CIV	10.0	\pm 1.1	915	\pm 442	59	\pm 8
HeII	4.8	0.6	658	456	32	4
CIII]	2.7	0.3	< 367	23	3	
NeIV	1.0	0.4	< 498	13	6	

1602-288

[NeV]	2.1	\pm 0.3	< 410	19	\pm 2
[OII]	19.0	1.9	< 358	189	20
[NeIII]	4.3	0.5	< 347	42	4
H γ	1.6	0.2	< 315	18	2
H β	0.8	0.3	< 274	18	2
[OIII]	10.8	1.1	< 270	179	25
[OIII]	38.4	3.8	< 267	649	93

1603+001

H α	26.0	\pm 4.8	1973	\pm 928	4	\pm 1
[SII]	6.3	2.9	< 853	1	1	

1621-115

[OII]	3.1	\pm 0.5	658	\pm 539	28	\pm 4
-------	-----	-----------	-----	-----------	----	---------

1628-268

[OII]	6.2	\pm 1.7	< 3222	86	\pm 32	
-------	-----	-----------	--------	----	----------	--

1643+022

[OII]	28.1	\pm 3.8	< 532	13	\pm 1	
[NeIII]	8.8	1.4	< 538	3	1	
H β	7.5	1.7	< 376	2	1	
[OIII]	102.1	10.3	< 367	27	2	
[OIII]	242.2	24.3	< 361	65	6	
H α	290.5	29.2	1911	283	86	8
[SII]	53.8	5.6	< 284	17	1	

Table 2. cont. Emission line properties.

Source & Line	Flux / 10^{-16} [erg/s/cm 2]	FWHM [km s $^{-1}$]	E.W. [Å]
---------------	------------------------------------	----------------------	----------

1643-223

CIII]	5.9	\pm 1.3	1400	\pm 938	38	\pm 11
CII]	5.6	1.3	3719	3537	13	3
MgII	32.5	3.9	6664	2345	76	10

1649-062

[OII]	4.9	\pm 1.2	< 853		39	\pm 11
-------	-----	-----------	-------	--	----	----------

1716+006

[NeV]	1.2	\pm 0.3	< 587		4	\pm 1
[OII]	4.2	0.5	412	335	15	1
[NeIII]	1.9	0.3	< 536		6	1
H γ	4.2	0.7	3473	626	15	2

1732-092

H β	140.9	\pm 14.1	4915	\pm 289	73	\pm 7
[OIII]	26.1	2.6	689	48	14	1
[OIII]	49.6	5.0	642	43	28	2
H α	187.0	19.0	5401	553	223	23

1810+046

CIII]	79.3	\pm 8.3	3109	\pm 706	22	\pm 2
NeIV	8.7	1.7	1251	865	1	1
MgII	207.0	20.9	6772	661	42	4

1912-269

[OII]	8.8	\pm 1.2	1149	\pm 602	48	\pm 7
[OIII]	3.2	0.5	< 336		11	1

1920-077

H β	1.4	\pm 0.5	< 314		27	\pm 1
[OIII]	5.8	0.7	502	177	120	67
[OIII]	19.2	2.0	539	72	401	232

2025-155

CIII]	3.7	\pm 0.5	2711	\pm 1379	24	\pm 4
CII]	2.6	0.3	1533	615	8	1
NeIV	2.5	0.3	1624	564	6	1

2120-166

CII]	1.6	\pm 0.8	< 817		11	\pm 6
MgII	7.3	1.9	< 6839		55	16
[OII]	12.4	1.3	728	306	168	38

2128-208

CIV	4.9	\pm 0.9	2041	\pm 1737	16	\pm 3
HeII	2.6	0.5	< 825		7	1
CIII]	9.2	1.1	4878	1839	21	2

2318-166

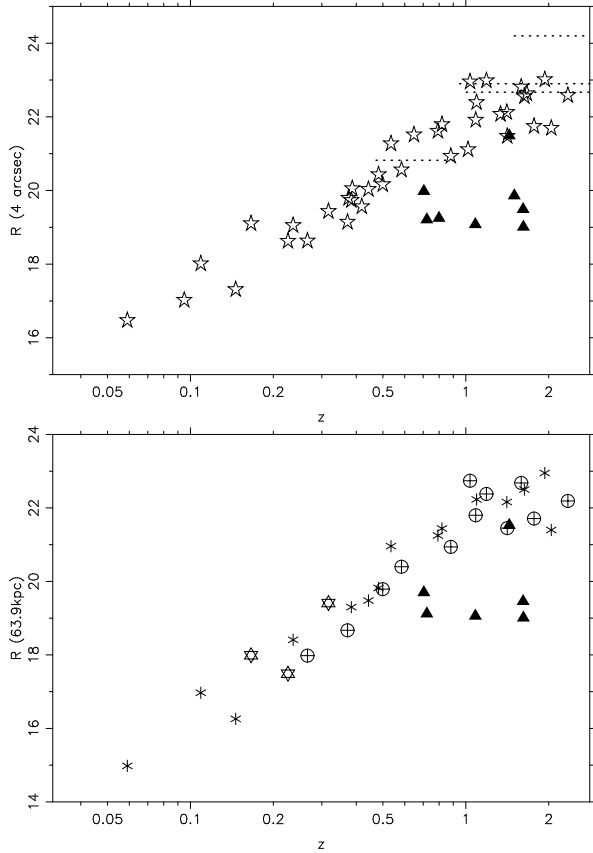


Figure 51. *R*-magnitude *vs* redshift diagrams. The upper plot shows the *R*-magnitude through a 4 arcsec diameter aperture, and includes all sources: the open stars represent radio galaxies and the filled triangles are quasars. The dotted lines depict the *R*-magnitudes of the 4 sources without redshifts. The lower plot shows the more physically-meaningful *R*-magnitude through a fixed 63.9 kpc aperture. The three types of open symbols represent the radio galaxies observed during the three different observing runs (asterisk — run 1; star — run 2; crossed circle — run 3), showing that there were no systematic differences between the different observing runs, and the filled triangles are the quasars.

tion of the host galaxy of each source have positional uncertainties typically well below 1 arcsecond. The 408 MHz flux density of the radio source is taken from the MRC catalogue value, except for radio sources of angular size larger than 100 arcseconds, in which case the Parkes Catalogue (Wright & Otrupcek 1990) value was used instead (see discussion in Section 5.2). The spectral index of the source was calculated between the 408 MHz flux density and the flux density at 1.4 GHz, the latter being determined from the NVSS catalogue (Condon et al. 1998). The radio power of each source, corrected to a rest-frame frequency of 408 MHz and calculated assuming $\Omega = 1$ and $H_0 = 50 \text{ km s}^{-1} \text{ Mpc}^{-1}$, is also tabulated.

The radio galaxies and quasars were classified, where observations of sufficient angular resolution were available for this to be done (otherwise they are classified as ‘U’), into three categories: Fanaroff and Riley (1974; hereafter FR) classes one (‘I’) and two (‘II’), and sources whose emission is dominated by the radio core, either as a core-jet or a core-halo source (‘C’). For a small number of sources,

complicated radio structure prohibits an unambiguous classification between FR Is and FR IIs; in these cases the classification is followed by a question mark to indicate the uncertainty, or designated as I/II. Determination of the angular size of the radio source depended upon the source classification. In the case of the majority FR II objects, the angular separation between the hotspots in each lobe most distant from the active nucleus was measured. For FR I’s and core dominated sources, the determined angular size is necessarily more arbitrary and less robust: whatever method is used the measured angular size of an FR I will always be highly dependent upon the sensitivity and frequency of the radio observations. In this paper, the maximum angular separation within the second highest radio contour on the quoted radio map was used.

The (heliocentric) redshifts of the host galaxies or quasars of the radio sources are provided in the table to an accuracy of three decimal places, unless the original measurement was not made to such precision, in which case it is given to the accuracy quoted in the original reference; uncertainties on the new redshifts presented in this paper can be found in Table 1. The nature of the host object is also classified in the table. Two sources lie nearby and are a starburst galaxy (NGC253) and a Seyfert 2 galaxy (NGC1068); the rest of the sources are classified as either a quasar or a radio galaxy. For the sources presented in this paper, a discussion of the classification scheme adopted has been presented in Section 4. Where possible this was also applied to the other 128 sources, but in the majority of cases it was only possible to accept the classification determined by the authors of the original imaging and spectroscopy papers. For some of the radio galaxies broad lines have been detected either in our spectroscopic observations (see Section 4) or in the literature, and these radio galaxies have been sub-classified as broad-line radio galaxies (BLRG’s). It should be noted, however, that some or many of the galaxies which remain classified under the more general ‘Radio Galaxy’ classification may actually be BLRG’s but the spectra are of insufficient quality to determine this.

Additionally provided in Table 3 are references to the optical identification, spectroscopic redshift, and a radio map of the galaxy. The optical identification reference refers to the publication which first identified the radio source host or to the first published finding chart of the field. The spectroscopic redshift is referenced by the first published value; for some sources later observations have confirmed this redshift and provided a more accurate value. Where this is the case the first publication is still given in the reference list, but the improved value for z is used. The third reference given is to a high quality radio map or, where none exist, the best radio data available in the literature. For sources which have been well-studied and have many radio maps in the literature, the reference is not necessarily to the most sensitive or the highest angular resolution data, but is simply to a map of sufficient quality to show clearly the important features of the radio source provided in the table.

Notes need to be added to the classifications and redshifts of three of these sources.

0347+052: The NASA/IPAC Extragalactic Database (NED) gives a redshift for this source of 0.76, but both Allington-Smith et al. (1991) and di Serego Alighieri et al.

(1994) derive a redshift of 0.339, and so the latter value is adopted here.

0834–196: This object is classified as a galaxy in NED, but di Serego Alighieri et al. (1994) point out that the host is actually an unresolved object, and they classify it as a quasar. That classification is adopted here.

2030–230: This object is classified as a quasar by Kapahi et al. (1998a), but in the rest of the literature is classified as an N-type galaxy. It is not sufficiently luminous to be classified as a quasar here, according to the classification scheme adopted in Section 4, and so falls within the radio galaxy population.

5.2 Radio selection effects: missing large sources?

An issue of concern in the definition of any sample of radio sources such as this is the possibility that giant radio sources, which may have sufficient flux density to be above the selection limit for the complete sample but owing to their large angular sizes may have only a low surface brightness, are missed from the sample. A discussion of this issue for the 3CR LRL sample can be found in Bennett (1962) and Riley (1989).

This issue indeed turns out to be very relevant for the MRC catalogue, due to the method of determining catalogue fluxes. As described by Large et al. (1981), the catalogue is based on a point-source fitting procedure, and so the flux density of sources whose angular size is comparable to or larger than the beam size (3 arcmins) may be systematically underestimated by an amount which depends strongly upon the angular structure of the source. To investigate how strong this effect is, for all of the radio sources in the BRL sample with angular sizes in excess of 60 arcsecs, the 408 MHz flux density from the MRC survey has been compared with that measured in the lower angular resolution Parkes Catalogue (Wright & Otrupcek 1990); the results are shown in Figure 52. The flux densities determined for the MRC sources are secure up to 100 arcsec, but above 200 arcsec the MRC flux densities of some sources are lower by as much as a factor of two (some of this difference may be due to the presence of other weaker sources within the large Parkes beam, but the majority is due to an underestimate of the MRC flux densities). Therefore, in Table 3 the flux densities quoted for sources larger than 100 arcsec are those taken from the Parkes Catalogue.

This result raises the possibility that some sources larger than ~ 200 arcsec have been missed from the sample because the MRC has underestimated their flux density, artificially placing them below the flux density cut-off. At high redshifts this effect is likely to be of little importance (200 arcsec corresponds to 1 Mpc at a redshift $z \approx 0.25$, and the 3CR sample shows that there are essentially no higher redshift sources larger than this size of sufficient flux density), but at $z = 0.1$ this angular size corresponds to only 500 kpc and below this redshift sources may be missed. Indeed, a comparison of the redshift distributions of the BRL and LRL samples[†] (Figure 53) shows that the BRL sample has a slightly lower peak at $z < 0.1$ which may be due to

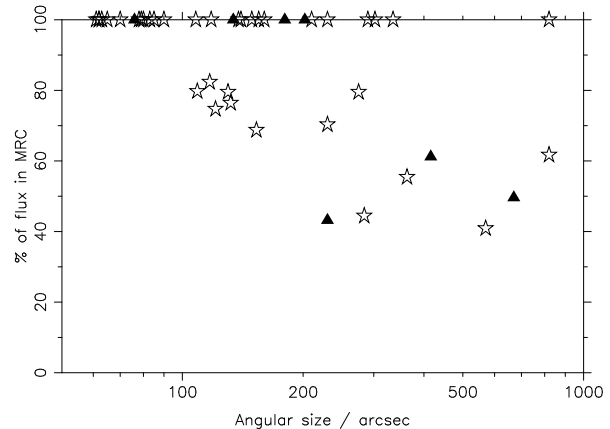


Figure 52. The percentage of the flux density in the 408 MHz Parkes Catalogue entry present in the MRC catalogue entry for all sources of angular size larger than 60 arcsec. The sources are separated into FR Is (filled triangles) and FR IIs (open stars).

this effect (although the combined counts at $z < 0.2$ are similar, and a Kolmogorov–Smirnov test shows no statistically significant differences between the two distributions). The BRL sample also contains a lower percentage of FR I class sources than the LRL sample, 8% as compared with 16%; FR Is enter the sample generally only at low redshifts and have considerable flux which can not be well-modelled as point sources, and so are perhaps more likely to be missed.

To summarise, whilst the sample is essentially complete at redshifts $z \gtrsim 0.2$, radio selection effects in the MRC catalogue may have led to a small number of low redshift sources with angular sizes $\gtrsim 200$ arcsec having been excluded from the sample.

5.3 Sample Properties

Some features of the sample can be easily examined and compared to those of the 3CR sample, to show any differences resulting from the selection at 408 MHz instead of 178 MHz. In Figure 54 is shown the radio power versus linear size ($P - D$) diagram for the BRL sample, and that for the LRL sample corrected to the same rest-frame frequency. In Figure 55 the redshift versus spectral index distribution of both samples is shown, showing the well-known increase in mean spectral index with redshift. The two samples show very similar distributions in both plots suggesting that there is little difference in their global properties. The mean and standard deviation of the spectral indices of the two samples are $\overline{\alpha}_{\text{BRL}} = 0.81 \pm 0.19$ and $\overline{\alpha}_{\text{LRL}} = 0.80 \pm 0.24$, both comparable. Figure 56 shows the distribution of sources from the two samples in the $D - \alpha$ plane; again the distributions are generally similar, although a small excess of BRL sources is to be found with small radio sizes ($D \lesssim 30$ kpc) and steep spectra ($\alpha \gtrsim 0.75$); it is not entirely unexpected that the higher selection frequency will select a larger fraction of these compact steep-spectrum sources, as synchrotron self-absorption prohibits these from entering low frequency

[†] Note: in accordance with the new observations of Willott et al. (1999), 3C318 in the LRL sample has been reclassified in our

diagrams as a quasar of redshift 1.574 instead of a radio galaxy at $z = 0.752$.

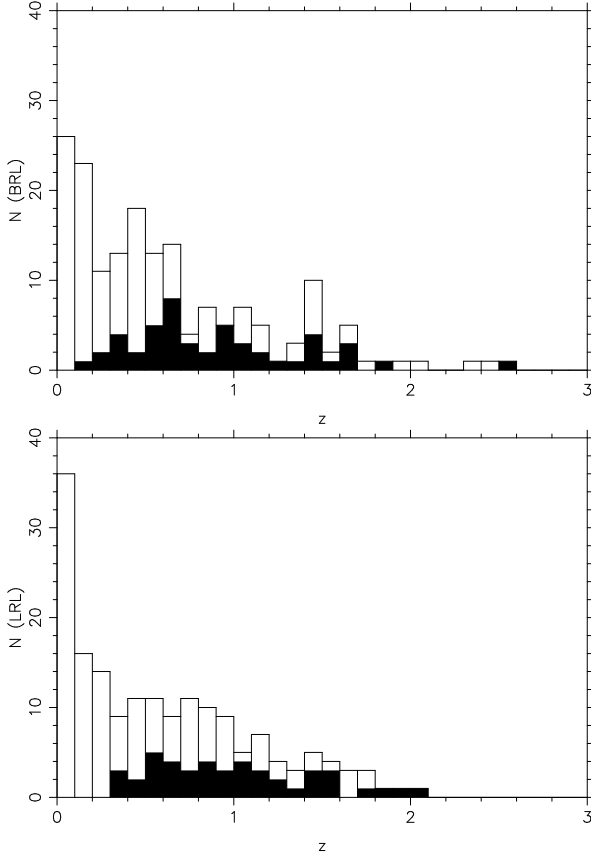


Figure 53. Top: A histogram of the redshift distribution of powerful radio sources in the BRL sample (shaded boxes represent quasars). Bottom: For comparison, the equivalent histogram for the 3CR sample of LRL.

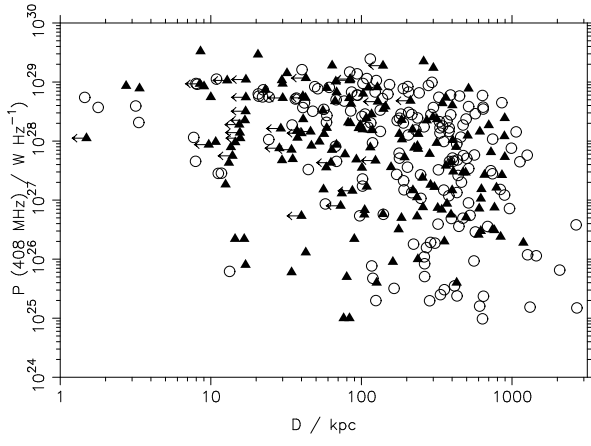


Figure 54. The radio power versus linear size ($P - D$) diagram for the BRL (filled triangles) and the LRL (open circles) sources.

selected samples. This appears to be the only important difference between the LRL and BRL samples.

The redshift distribution of the two samples has already been shown to be similar in Figure 53. An interesting feature of this plot is that the fraction of radio galaxies and quasars at redshifts $z \gtrsim 1.5$ in the new BRL sample remains roughly constant, indicating that the 100% quasar fraction beyond $z = 1.8$ in the LRL sample is just due to small number

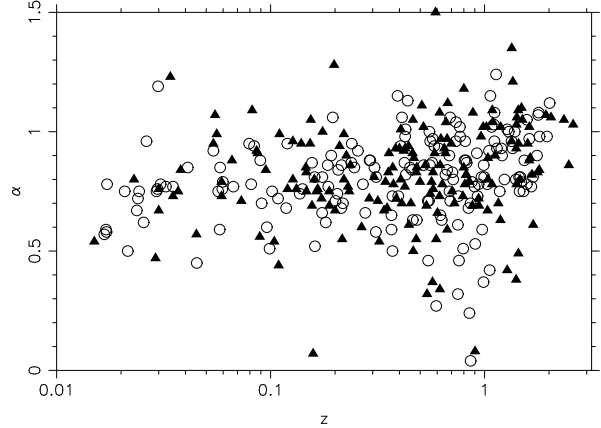


Figure 55. The spectral index versus redshift distribution of the BRL (filled triangles) and LRL (open circles) sources.

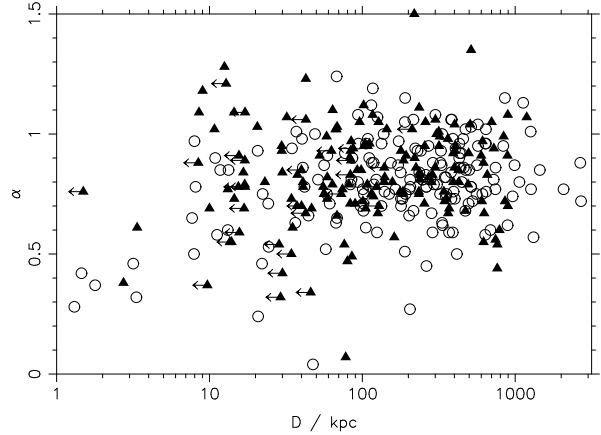


Figure 56. The spectral index versus linear size distribution of the BRL (filled triangles) and LRL (open circles) sources.

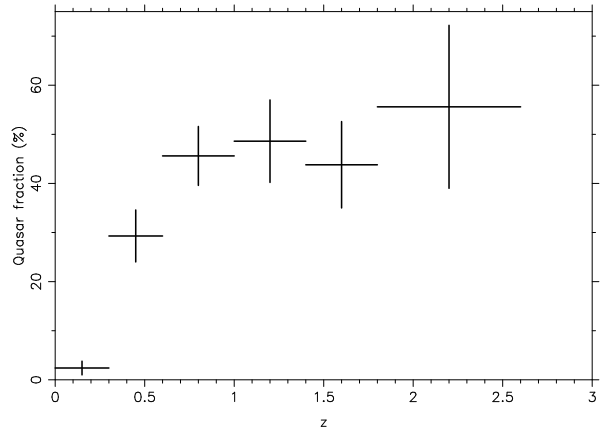


Figure 57. The quasar fraction as a function of redshift from the combined BRL and LRL samples. Note that inclusion of the four radio galaxies from the BRL sample without determined redshifts would slightly decrease the high redshift quasar fractions, but by much less than the size of the error bars.

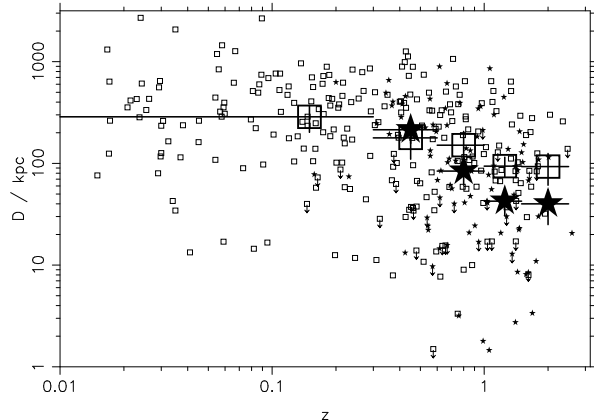


Figure 58. The linear size versus redshift distribution for the BRL and LRL samples, split into radio galaxies (open squares) and quasars (filled stars). The larger points with error bars correspond to the median values in five different redshift ranges. No point is plotted for the quasars with $0 < z < 0.3$ due to the small number (3) of quasars in this redshift range.

statistics. This result can be seen in Figure 57 which shows the quasar fraction as a function of redshift from the combined BRL and LRL samples; there is no significant increase in the quasar fraction at the highest redshifts. Both samples show a stark lack of quasars at the lowest redshifts, which has been discussed by many authors. In orientation-based unification schemes (e.g. Barthel 1989) this is partially attributed to broad-line radio galaxies being the equivalent of the quasar population at low redshifts (e.g. see Antonucci 1993 for a review); more sophisticated explanations have been proposed, including an evolution in the opening angle of the torus with radio power (e.g. Lawrence 1991), or the presence of an isotropic population of low excitation radio galaxies at low redshift (Laing et al. 1994).

The simple unification scheme of Barthel (1989) makes strong predictions for the relative linear sizes of radio galaxies and quasars; indeed, the difference in linear sizes between the two populations in the 3CR sample was one of the factors which led him to propose the model. Figure 58 now shows the radio size versus redshift distribution for the BRL and LRL samples combined, plotting radio galaxies and quasars separately. The median linear sizes of the radio galaxies and quasars have been calculated in five separate redshift bins, the lowest redshift bin including insufficient quasars to calculate an accurate median. With the increased number of sources, the result of Barthel (1989) still holds that radio galaxies with $0.5 < z < 1.0$ are, on average, larger than quasars in the same redshift range by about a factor of two. This relation is also true for higher redshifts, but the larger number statistics confirm that the result does not hold at lower redshifts (e.g. see Singal et al. 1993 for the LRL sample alone; although cf. the discussion of Section 5.2 which might have a slight effect here). Again, this rules out the simplest unification schemes, but can plausibly be explained by the modifications discussed above (e.g. see Gopal-Krishna et al. 1996).

6 CONCLUSIONS

Details of a new sample of the most powerful equatorial radio sources have been collated. New radio imaging, optical imaging and spectroscopic observations have been presented of the sources previously without spectroscopic redshifts, leading to the complete sample being fully optically identified and spectroscopic redshifts being available for 174 of the 178 sources (98%). Work to obtain the redshifts for the remaining four sources is continuing.

Due to method of determining flux densities used for the Molonglo Reference Catalogue, radio selection effects may have led to a small number of radio sources subtending angular sizes larger than about 200 arcseconds being missed from the catalogue; this probably gives rise to the slightly lower percentage of FRI sources in the new sample of radio sources as compared with the revised 3CR sample. Another observed difference is that the new sample contains a higher percentage of compact steep spectrum sources than the 3CR sample; this was to be expected since these sources are often missed in low frequency selected samples due to synchrotron self-absorption. No other significant differences are found between the properties of the new sample and those of the 3CR sample.

Due to its equatorial location and its high spectroscopic completeness, this sample will prove very useful for studies using a combination of the northern hemisphere instruments such as the VLA, and the new and forthcoming southern hemisphere telescope facilities, such as the large optical telescopes and the Atacama Large Millimetre Array.

ACKNOWLEDGEMENTS

This work was supported in part by the Formation and Evolution of Galaxies network set up by the European Commission under contract ERB FMRX- CT96-086 of its TMR programme. This work is based upon observations made at the European Southern Observatory, La Silla, Chile, and using the William Herschel Telescope and the Very Large Array. The William Herschel Telescope is operated on the island of La Palma by the Isaac Newton Group in the Spanish Observatorio del Roche de los Muchachos of the Instituto de Astrofisica de Canarias. The National Radio Astronomy Observatory is operated by Associated Universities Inc., under co-operative agreement with the National Science Foundation. The Digitized Sky Surveys were produced at the Space Telescope Science Institute under U.S. Government grant NAG W-2166. This research has made use of the NASA/IPAC Extragalactic Database (NED) which is operated by the Jet Propulsion Laboratory, California Institute of Technology, under contract with the National Aeronautics and Space Administration. The authors thank Jaron Kurk for his work with the VLA archive data, and the referee, Steve Rawlings, for a very careful consideration of the manuscript and a number of helpful suggestions.

REFERENCES

- Adams T. F., 1977, ApJ Supp., 33, 19 [ada77]
- Adgie R. L., 1964, Nat, 204, 1028 [adg64]
- Aldcroft T. L., Elvis M., Bechtold J., 1993, AJ, 105, 2054 [ald93]

Table 3: Properties of the BRL sample of radio sources. The columns give the source name, the right ascension, declination and galactic latitude of the optical ID, the integrated flux density at 408 MHz, the spectral index between 408 MHz and 1.4 GHz, the radio power at a rest-frame wavelength of 408 MHz (assuming $\Omega = 1$ and $H_0 = 50 \text{ km s}^{-1} \text{ Mpc}^{-1}$), the largest angular size of the radio source and its morphological classification, the redshift of the host galaxy or quasar, the nature of the host object, common alternative names for the source, and references to the optical identification of the host galaxy or quasar, the spectroscopic redshift, and a radio map.

Source	RA	Dec	b	S_{408} [Jy]	α_{1400}^{408}	P_{408} [$10^{27} \text{ W Hz}^{-1}$]	D [']	Morph.	z	ID ¹	Other names	References ²		
												Opt ID	z	Radio
0000-177	00 00 48.55	-17 43 56.4	-75	6.51	0.80	74.4	2.7	II	1.465	Q		hun78	hun78	ald93
0003-003	00 03 48.91	-00 21 06.5	-60	10.45	0.80	57.6	4.8	II	1.037	Q	3C2	san65a	lyn67	sai87
0016-129	00 16 18.84	-12 59 13.7	-73	6.87	0.95	107.5	3.5	II	1.589	RG		brl	brl	brl
0020-253	00 20 38.13	-25 19 07.0	-83	5.36	0.68	2.94	79	II	0.35	RG		mcc96	mcc96	kap98a
0022-297	00 22 00.24	-29 45 31.6	-83	7.83	0.80	6.06	44	II	0.406	Q		bol65	sti93a	kap98b
0023-263	00 23 18.96	-26 18 49.5	-84	17.00	0.54	7.57	< 5	U	0.322	RG		pre83	tad93	mor93
0032-203	00 32 38.60	-20 20 30.9	-82	6.87	1.02	9.68	1.5	II	0.518	RG		mcc96	mcc96	kap98a
0034-014	00 34 30.59	-01 25 38.6	-63	9.74	0.71	0.22	48	II	0.073	RG	3C15	haz65	bur67	lea97
0035-024	00 35 47.17	-02 24 09.3	-64	16.53	0.80	3.62	35	I/II	0.220	BLRG	3C17	wyn66	sch65	mor93
0038+097	00 38 14.76	09 46 59.5	-52	11.54	0.75	22.8	46	II	0.188	RG	3C18	wyn66	smi80a	mor93
0045-255	00 45 05.74	-25 33 39.6	-88	6.12	0.58	0.00002	26		0.0008	SB	NGC253	eva57	bur62	mor93
0051-038	00 51 35.57	-03 50 11.3	-66	7.03	0.94	1.44	< 20	U	0.210	RG	3C26	bol66b	sch65	con98
0055-016	00 55 01.57	-01 39 39.7	-64	10.88	0.57	0.09	134	II?	0.045	RG	3C29	wyn66	san67	mor93
0056-172	00 56 37.93	-17 16 50.0	-79	6.21	1.02	38.6	17	II	1.019	RG		brl	brl	brl
0101-128	01 01 52.91	-12 51 18.8	-75	5.18	0.72	3.54	16	II	0.387	RG		brl	brl	brl
0105-163	01 05 48.74	-16 20 20.4	-79	13.24	0.93	10.4	63	II	0.400	RG	3C32	pre83	tad93	mor93
0114-211	01 14 25.98	-21 07 55.3	-81	10.64	0.78	110.2	< 2	U	1.41	RG		dis94	mcc96	kap98a
0115+027	01 15 43.64	02 42 19.8	-59	6.07	1.12	15.8	13	II	0.672	Q	3C37	bol68	sea68	hut98
0116+082	01 16 24.25	08 14 09.5	-53	5.20	0.55	7.9	1.8	C	0.594	RG	4C08.06	spi76	spi76	coh97
0117-155	01 17 59.66	-15 36 00.9	-76	13.52	0.79	20.7	11	II	0.565	RG	3C38	fug88	tad93	mor93
0125-143	01 25 02.65	-14 18 27.2	-74	7.43	0.85	4.88	15	II	0.372	RG		brl	brl	brl
0128+061	01 28 45.20	06 08 15.0	-55	5.15	1.04	12.4	65	II	0.660	RG	3C44	cla66	spi85b	bog94
0128-264	01 28 06.63	-26 25 23.8	-81	5.36	1.05	224.3	33	II	2.348	RG		mcc96	brl	brl
0132+079	01 32 37.49	07 55 47.5	-53	5.99	0.79	7.09	9	II	0.499	RG	3C45	brl	brl	brl
0139-273	01 39 07.90	-27 21 18.5	-79	5.04	0.95	63.5	12	II	1.44	RG		mcc96	mcc96	kap98a
0148-297	01 48 19.59	-29 46 46.3	-76	7.04	0.70	5.38	138	II	0.41	RG		mcc96	mcc96	kap98a
0155-109	01 55 14.06	-10 58 16.6	-67	5.36	0.73	9.56	1.9	II	0.616	Q		bol66c	bur68	ald93
0159-117	01 59 30.35	-11 46 59.0	-67	5.70	0.59	11.2	< 2	U	0.669	Q	3C57	bol66b	sea68	ald93
0213-132	02 13 12.35	-13 13 25.4	-65	11.73	0.75	1.12	70	II	0.147	RG	3C62	pre83	tad93	mor93
0218-021	02 18 21.94	-02 10 32.7	-56	11.77	1.00	1.67	80	II	0.175	RG	3C63	wyn66	smi80a	hav98
0219+082	02 19 19.16	08 13 26.3	-48	5.29	0.60	1.63	155	II	0.266	RG	3C64	brl	brl	brl
0222-234	02 22 45.99	-23 26 19.6	-68	5.44	0.77	1.30	16	II	0.230	Q		kap98b	bak95	kap98b
0235-197	02 35 24.76	-19 45 30.8	-64	13.27	0.86	25.5	39	II	0.620	RG		pre83	tad93	mor93
0240-002	02 40 07.06	-00 13 31.4	-51	12.36	0.77	0.0008	~ 60		0.004	Sy2	3C71,NGC1068	mil55	hum56	gal96
0254-236	02 54 01.27	-23 36 59.8	-61	5.87	1.11	8.26	33	II	0.509	RG		mcc96	mcc96	kap98a
0255+058	02 55 03.05	05 49 37.0	-44	16.20	0.80	0.04	670	I	0.023	RG	3C75	mal63	mal63	owe85
0305+039	03 05 49.09	03 55 13.2	-44	13.60	0.47	0.05	100	I	0.029	RG	3C78,NGC1218	mal63	sch65	bau88
0310-150	03 10 25.90	-15 01 03.5	-54	6.10	0.83	107.0	< 10	U	1.769	RG		brl	brl	brl
0320+053	03 20 41.54	05 23 34.6	-40	7.13	0.76	11.2	< 0.2	U	0.575	RG	4C05.14	cla66	hec94	man97
0325+023	03 25 18.19	02 23 20.3	-42	10.90	0.67	0.04	153	II	0.030	RG	3C88	wyn66	sch65	bau88
0331-013	03 31 43.01	-01 20 55.9	-43	8.66	0.95	0.76	80	I	0.139	RG	3C89	wyn66	smi76c	bau88
0340+048	03 40 51.54	04 48 21.7	-37	8.65	0.91	5.31	32	II	0.357	Q	3C93	san65b	smi80b	bog94
0347+057	03 47 07.07	05 42 38.1	-35	7.47	0.67	3.83	62	II	0.339	BLRG	4C05.16	fug88	all91	mor93

Table 3: **cont.** Properties of the BLR sample of radio sources.

Source	RA	Dec	b	S_{408} [Jy]	α_{1400}^{408}	P_{408} [10^{27} W Hz $^{-1}$]	D ["]	Morph.	z	ID ¹	Other names	References ²		
												Opt ID	z	Radio
B1950														
0349-146	03 49 09.46	-14 38 05.4	-46	11.60	1.08	24.5	117	II	0.616	Q	3C95	bol66d	sch66	bog94
0349-278	03 49 31.85	-27 53 30.4	-50	15.80	0.88	0.30	363	II	0.066	RG		bol65	sea68	mor93
0350-073	03 50 04.02	-07 19 55.8	-42	10.22	0.98	54.3	43	II	0.962	Q	3C94	bol66d	lyn67	swa86
0357-163	03 57 59.79	-16 18 36.2	-45	5.65	0.91	9.81	7.0	II	0.584	RG		brl	brl	brl
0358+004	03 58 33.31	00 28 10.8	-36	5.29	0.93	4.74	4.5	II	0.426	RG	3C99	kri74	smi76a	man97
0403-132	04 03 13.95	-13 16 18.4	-42	6.70	0.37	8.69	< 1.3	U	0.571	Q		bol66d	lyn67	hut98
0404+035	04 04 38.98	03 34 27.3	-33	9.35	0.56	0.32	335	II	0.089	RG	3C105	smi76b	smi80a	lea97
0405-123	04 05 27.46	-12 19 31.9	-41	8.17	0.83	13.2	32	II	0.574	Q		kin66	kin67a	mor93
0406-180	04 06 52.13	-18 05 01.1	-43	5.60	0.70	13.6	< 5	U	0.722	Q		brl	brl	brl
0413-210	04 13 53.62	-21 03 51.0	-43	7.30	0.78	23.5	5.0	II	0.808	Q		sav76	wri83	kap98b
0430+052	04 30 31.61	05 14 59.5	-27	6.08	0.36	0.03	850	I	0.033	BLRG	3C120	wee76	ada77	wal87
0442-282	04 42 37.81	-28 15 22.6	-38	18.85	0.83	1.82	86	II	0.147	RG		pre83	tad93	kap98a
0453-206	04 53 14.08	-20 38 58.9	-34	11.25	0.73	0.06	36	II?	0.035	RG	NGC1692	bol65	mcc96	mor93
0508-220	05 08 53.17	-22 05 32.6	-31	5.10	0.80	0.58	39	II	0.16	RG		dri97	dri97	kap98a
0511+008	05 11 33.58	00 53 07.7	-21	8.00	0.80	0.57	132	II	0.127	BLRG	3C135	wyn66	san67	lea97
0519-208	05 19 30.13	-20 50 30.8	-28	7.34	1.09	55.2	< 2	U	1.086	RG		brl	brl	brl
0528+064	05 28 48.10	06 28 14.8	-14	11.19	1.01	9.31	49	II	0.406	RG	3C142.1	hes96	hew91	bog94
0604-203	06 04 24.69	-20 21 35.9	-18	7.39	0.75	0.80	< 20	U	0.164	RG		mer69	wri90	con98
0634-205	06 34 23.27	-20 32 18.3	-12	22.70	1.07	0.19	820	II	0.055	RG		bol65	sea68	bau88
0806-103	08 06 30.29	-10 18 50.2	12	13.70	0.99	0.74	121	II	0.110	RG	3C195	bol66b	tad93	mor93
0812-029	08 12 57.09	-02 59 12.1	17	9.54	1.28	1.84	3.0	C	0.198	RG	3C196.1	wyn66	smi76c	nef95
0825-202	08 25 03.54	-20 16 27.7	10	10.27	0.82	35.1	17	II	0.822	Q		bol66b	dis94	mor93
0834-196	08 34 56.07	-19 41 25.4	12	10.84	0.67	53.9	< 5	U	1.032	Q		fug88	dis94	mor93
0850-206	08 50 45.02	-20 36 03.3	15	7.49	0.96	80.8	13	II	1.337	BLRG		brl	brl	brl
0851-142	08 51 27.81	-14 16 28.2	18	5.19	0.82	79.3	7.0	II	1.665	RG		brl	brl	brl
0859-257	08 59 36.40	-25 43 26.0	13	17.17	0.81	7.38	43	II	0.305	RG		dis94	tad93	mor93
0915-118	09 15 41.19	-11 53 04.9	25	132.00	0.95	1.69	76	I	0.054	RG	3C218,Hydra A	bol66b	hum56	mor93
0933+045	09 33 55.17	04 35 38.7	38	5.13	1.35	77.4	60	II	1.339	RG	3C222	djo88	hec94	law95
0945+076	09 45 06.53	07 39 17.4	42	15.53	0.92	0.51	230	II	0.086	BLRG	3C227	wyn66	san67	bla92
0949+002	09 49 25.12	00 12 36.8	39	12.30	1.10	190.6	7.5	II	1.487	RG	3C230	ham90	hew91	rhe96
1002-215	10 02 50.28	-21 30 16.0	26	6.71	1.50	15.7	29	II	0.59	RG		mcc96	mcc96	kap98a
1005+077	10 05 22.04	07 44 58.6	46	15.35	0.69	55.5	1.2	II	0.877	RG	3C237	bol66a	spi85a	nan91
1008+066	10 08 23.10	06 39 26.5	46	9.32	0.93	109.3	9.8	II	1.405	RG	3C238	smi76b	spi84	law86
1039+029	10 39 04.10	02 58 14.6	50	6.38	0.69	8.37	6.4	II	0.535	RG	4C03.18	brl	brl	brl
1048-090	10 48 59.41	-09 02 13.6	43	5.35	0.79	2.93	83	II	0.344	Q	3C246	bol66e	kin67a	hut98
1059-010	10 59 30.46	-01 00 06.6	51	8.04	0.86		22	II		RG	3C249	brl	brl	brl
1103-208	11 03 54.36	-20 52 47.1	35	7.64	0.90	53.4	9.7	II	1.12	RG		mcc96	mcc96	kap98a
1116-027	11 16 52.14	-02 46 26.1	52	7.73	1.21	106.5	< 1.5	U	1.355	Q	3C255	djo88	gir90	rhe96
1120+057	11 20 34.24	05 46 48.7	59	5.08	0.86	189.0	< 18	U	2.474	RG	3C257	hew91	hew91	con98
1127-145	11 27 35.67	-14 32 54.3	43	5.07	-0.08	18.7	0.01	C	1.187	Q		bol66e	bur66	kel98
1131-171	11 31 52.37	-17 11 14.5	41	5.87	1.02	102.2	8.0	II	1.618	Q		brl	brl	brl
1136-135	11 36 38.51	-13 34 05.9	45	10.50	0.74	15.3	16	II	0.557	Q		bol66e	kin67a	bog94
1138+015	11 38 34.45	01 30 56.9	59	5.72	0.61	4.95	5.2	II	0.443	RG	4C01.32	brl	brl	brl
1139-285	11 39 03.61	-28 34 09.7	31	6.81	0.79	24.5	13	II	0.85	RG		mcc96	mcc96	kap98a
1140-114	11 40 02.37	-11 25 09.4	47	5.14	1.07	141.4	3.9	II	1.935	BLRG		brl	brl	brl
1216+061	12 16 49.90	06 06 08.8	67	41.50	0.71	0.01	416	I	0.007	RG	3C270,NGC4261	mal63	hum56	mor93
1216-100	12 16 03.40	-10 03 55.6	51	7.70	0.91	0.26	275	II	0.087	RG		dan83	dan83	con98
1226+023	12 26 33.25	02 19 43.3	64	59.75	0.07	5.97	22	C	0.158	Q	3C273	haz63	sch63	dav91

Table 3: **cont.** Properties of the BLR sample of radio sources.

Source	RA	Dec	b	S_{408} [Jy]	α_{1400}^{408}	P_{408} [10^{27} W Hz $^{-1}$]	D ["]	Morph.	z	ID ¹	Other names	References ²		
												Opt ID	z	Radio
B1950														
1232-249	12 32 59.35	-24 55 45.7	37	5.10	0.83	2.68	109	II	0.355	Q		bol66f	bur69	kap98b
1239-044	12 39 45.10	-04 29 51.0	58	10.24	0.83	11.4	5.4	II	0.480	RG	3C275	kri74	spi79	man97
1245-197	12 45 45.23	-19 42 57.5	42	8.61	0.42	53.7	< 3.5	U	1.275	Q		wal80	dis94	mor93
1252-122	12 51 58.56	-12 17 52.2	50	14.70	0.54	0.01	180	I	0.015	RG	3C278,NGC4783	vor59	dah85	mor93
1253-055	12 53 35.84	-05 31 08.1	57	14.45	0.32	16.3	< 4	U	0.538	Q	3C279	san65b	bur65a	hut98
1303+091	13 03 05.12	09 11 18.5	71	5.21	1.03	67.1	8.0	II	1.409	RG	4C09.45	brl	brl	brl
1306-095	13 06 02.09	-09 34 33.3	52	7.84	0.50	7.15	< 5	U	0.464	RG		pre83	tad93	mor93
1307+000	13 07 16.00	00 03 22.2	62	5.10	0.92	4.40	60	II	0.419	RG	4C00.46	brl	brl	brl
1308-220	13 08 57.37	-22 00 46.2	40	22.21	1.18	84.6	1.1	U	0.8	RG	3C283	mcc96	mcc96	kap98a
1327-214	13 27 23.38	-21 26 33.9	40	5.63	0.86	7.72	31	II	0.528	Q		bol65	bur66	ald93
1330+022	13 30 20.47	02 16 08.8	63	5.29	0.55	1.06	140	II	0.216	BLRG	3C287.1	wyn66	san66	hav98
1335-061	13 35 31.20	-06 11 56.7	54	9.74	0.97	20.1	11	II	0.625	Q	4C-06.35	san65b	bur66	bog94
1344-078	13 44 23.60	-07 48 25.2	52	5.98	0.93	4.30	< 10	U	0.384	RG		brl	brl	brl
1354+013	13 54 28.53	01 19 17.4	59	6.59	0.82	22.4	33	II	0.819	RG	4C01.39	brl	brl	brl
1411-057	14 11 11.18	-05 45 58.9	51	5.49	1.04	40.4	47	II	1.094	RG	4C-05.60	brl	brl	brl
1413-215	14 13 52.46	-21 32 20.1	36	5.57	1.11		19	II		RG		brl	brl	brl
1416+067	14 16 38.78	06 42 20.9	60	23.36	1.09	331.3	1.0	II	1.436	Q	3C298	adg64	lyn66	ald93
1417-192	14 17 02.63	-19 14 41.8	38	5.02	0.76	0.32	62	II	0.120	RG		bol66b	hun78	ant85
1419-272	14 19 55.15	-27 14 20.0	31	8.36	1.02	48.1	< 25	U	0.985	Q		wro81	ver96	con98
1422-297	14 22 32.91	-29 46 25.1	28	7.17	0.89	112.3	< 10	U	1.632	RG		brl	brl	brl
1425-011	14 25 56.64	-01 10 44.6	53	7.21	0.70	46.5	< 15	U	1.159	RG	3C300.1	djo88	djo88	con98
1434+036	14 34 26.14	03 37 11.5	55	5.16	0.49	43.0	10	II	1.438	Q	4C03.30	brl	brl	brl
1436-167	14 36 42.08	-16 46 10.0	38	5.61	0.85	0.54	< 12	U	0.146	BLRG		brl	brl	brl
1452-041	14 52 24.22	-04 08 52.8	46	6.72	0.94	6.50	108	II	0.441	RG	3C306.1	wyn66	smi80a	hav98
1453-109	14 53 12.22	-10 56 39.9	41	10.33	0.72	43.8	41	II	0.938	Q		haz64	sch66	mil78
1508+080	15 08 33.04	08 02 58.5	51	11.50	0.91	12.1	130	II	0.461	RG	3C313	wyn65	smi80a	bog94
1508-055	15 08 14.93	-05 31 47.9	42	7.72	0.63	49.4	0.02	C	1.185	Q	4C-05.64	kri70	pet72	kel98
1509+015	15 09 52.90	01 32 20.6	47	5.56	0.73	16.7	7.2	II	0.792	RG	4C01.42	brl	brl	brl
1514+072	15 14 16.99	07 12 17.1	50	25.18	1.23	0.13	46	C	0.034	RG	3C317	mat64	sch65	mor93
1524-136	15 24 12.84	-13 40 31.1	34	6.11	0.61	78.0	0.4	U	1.687	Q		bol66b	hew93	man92
1600+021	15 59 55.64	02 06 12.8	37	16.11	0.54	0.75	302	II	0.104	RG	3C327	mal63	sch65	lea97
1602+014	16 02 12.96	01 25 58.7	37	14.87	1.05	16.6	14	II	0.462	RG	3C327.1	jau89	spi85a	bog94
1602-093	16 02 47.21	-09 19 24.0	30	6.08	0.44	0.31	290	II	0.109	RG		brl	brl	brl
1602-174	16 02 09.55	-17 26 10.9	25	5.64	1.06	173.7	37	II	2.043	RG		brl	brl	brl
1602-288	16 02 06.65	-28 51 05.2	17	7.07	0.85	7.97	61	II	0.482	RG		brl	brl	brl
1603+001	16 03 39.05	00 08 29.7	36	5.61	0.79	0.08	11	I	0.059	RG	4C00.58	brl	brl	brl
1621-115	16 21 13.22	-11 33 50.5	25	7.15	0.78	4.67	< 20	U	0.375	RG		brl	brl	brl
1628-268	16 28 36.47	-26 50 28.8	14	5.66	0.76	0.69	93	II	0.166	RG		brl	brl	brl
1643+022	16 43 11.13	02 17 09.4	28	5.52	0.84	0.22	7.1	II	0.095	RG	4C02.42	brl	brl	brl
1643-223	16 43 05.02	-22 22 40.6	14	5.68	0.85	18.6	12	II	0.799	Q		brl	brl	brl
1648+050	16 48 39.98	05 04 35.1	28	169.50	1.05	18.6	202	I/II	0.154	RG	3C348, Herc A	mal63	gre62	hav98
1649-062	16 49 00.30	-06 13 13.8	23	5.73	0.86	1.47	85	II	0.236	RG		brl	brl	brl
1716+006	17 16 49.94	00 40 10.6	20	5.54	0.75	13.2	7.1	II	0.704	Q		brl	brl	brl
1717-009	17 17 53.28	-00 55 48.7	19	138.00	0.76	0.53	284	II	0.030	RG	3C353	mal63	sch65	swa96
1730-130	17 30 13.53	-13 02 45.8	10	6.58	0.08	17.0	0.03	C	0.902	Q		kri70	jun84	she97
1732-092	17 32 23.74	-09 14 43.8	12	5.30	0.71	2.40	45	II	0.317	BLRG		brl	brl	brl
1810+046	18 10 47.67	04 38 39.1	10	5.51	0.78	32.8	6.5	II	1.083	Q	4C04.63	brl	brl	brl
1859-235	18 59 47.44	-23 34 16.2	-12	10.92	0.88		4.2	II		RG		brl	brl	brl

Table 3: **cont.** Properties of the BLR sample of radio sources.

Source	RA	Dec	b	S_{408} [Jy]	α_{1400}^{408}	P_{408} [$10^{27} \text{ W Hz}^{-1}$]	D ['']	Morph.	z	ID ¹	Other names	References ²
B1950												
1912-269	19 12 42.75	-26 58 16.2	-16	6.21	0.90	1.47	48	II	0.226	RG		Opt ID
1920-077	19 20 48.42	-07 47 30.1	-10	6.04	0.93	13.2	23	II	0.648	RG		z
1921-293	19 21 42.24	-29 20 26.4	-19	5.63	-0.70	2.06	0.01	C	0.352	Q		Radio
1938-155	19 38 24.60	-15 31 33.9	-17	16.00	0.70	14.9	5.5	II?	0.452	RG		
1949+023	19 49 44.54	02 22 37.8	-12	13.57	0.73	0.20	230	II	0.059	RG	3C403	wyn65
1953-077	19 53 29.45	-07 44 57.9	-17	5.88	0.96		4.3	II		RG	3C404	brl
2019+098	20 19 44.14	09 51 33.0	-15	10.00	0.89	10.7	27	II	0.467	BLRG	3C411	spi75
2025-155	20 25 19.17	-15 31 20.5	-28	5.41	1.05	81.7	15	II	1.500	Q		brl
2030-230	20 30 20.50	-23 03 33.6	-32	6.45	0.76	0.50	70	II	0.132	RG		brl
2044-027	20 44 34.21	-02 47 25.8	-26	5.37	0.69	22.5	< 2	U	0.942	Q	3C422	bra74
2045+068	20 45 44.36	06 50 09.8	-22	7.86	0.96	0.57	35	II	0.127	RG	3C424	wyn65
2053-201	20 53 12.98	-20 08 08.1	-36	6.37	0.69	0.68	30	II	0.156	RG		smi80b
2058-282	20 58 38.68	-28 13 43.9	-39	15.90	0.84	0.10	230	I?	0.038	RG	NGC6998	smi80a
2104-256	21 04 29.87	-25 37 50.2	-40	13.25	0.75	7.81	114	II	0.037	RG	NGC7018	bla92
2111-259	21 11 44.79	-25 54 19.4	-41	5.27	0.66	8.68	9.0	II	0.602	Q		haz72
2113-211	21 13 45.42	-21 08 16.8	-40	9.05	0.95	23.5	40	II	0.698	RG		sti93b
2120-166	21 20 15.39	-16 40 47.4	-40	6.09	1.08	28.5	14	II	0.882	RG		kap98a
2128-208	21 28 12.27	-20 50 09.7	-44	6.15	0.88	93.2	< 1	U	1.615	Q		brl
2135-147	21 35 01.15	-14 46 27.4	-43	8.78	0.67	1.54	149	II	0.200	Q		brl
2135-209	21 35 01.34	-20 56 03.0	-45	9.76	0.78	19.0	< 2	U	0.635	RG		brl
2146-133	21 46 46.35	-13 18 26.4	-45	5.10	0.84	93.8	3.6	II	1.800	Q		brl
2149-200	21 49 04.35	-20 00 10.8	-48	5.12	0.77	4.29	2.0	II?	0.424	Q		brl
2149-287	21 49 10.56	-28 42 36.9	-50	5.68	0.55	5.62	< 2	U	0.479	RG		brl
2154-184	21 54 12.13	-18 28 03.7	-49	6.09	0.97	14.5	78	II	0.668	Q		brl
2203-188	22 03 25.73	-18 50 17.1	-51	9.73	0.34	14.5	< 6	U	0.618	Q		brl
2211-172	22 11 42.71	-17 16 31.4	-52	28.66	0.95	3.05	118	II	0.153	RG	3C444	wyn65
2216-281	22 16 53.51	-28 11 32.1	-56	6.24	0.91	13.9	< 2	U	0.657	RG		mcc96
2221-023	22 21 14.66	-02 21 26.8	-46	17.50	0.99	0.24	570	II	0.056	BLRG	3C445	wyn66
2223-052	22 23 11.12	-05 12 17.4	-48	11.89	0.38	85.9	0.32	C	1.404	Q	3C446	sch65
2309+090	23 09 56.59	09 03 06.9	-46	6.25	0.75	1.52	12	II	0.233	RG	3C456	fej92
2310+050	23 10 21.90	05 00 26.0	-49	7.08	0.72	2.66	160	II	0.289	RG	3C458	wyn66
2314+038	23 14 02.34	03 48 55.0	-51	15.78	0.99	3.59	13	II	0.220	BLRG	3C459	hav98
2317-277	23 17 15.46	-27 43 50.0	-69	5.44	0.72	0.72	160	II	0.173	RG		bol65
2318-166	23 18 24.77	-16 39 32.5	-66	8.75	1.06	116.7	< 5	U	1.414	RG		brl
2322-052	23 22 45.08	-05 14 06.9	-59	5.43	1.02	47.4	7.8	II	1.188	RG	4C-05.96	brl
2322-123	23 22 43.66	-12 23 57.0	-64	7.20	1.09	0.22	7.0	U	0.082	RG		brl
2324-023	23 24 19.66	-02 18 45.1	-57	5.57	0.69	0.87	92	U	0.188	RG		bol66b
2338+042	23 38 24.66	04 14 37.2	-54	5.70	1.03	291.9	2.7	II	2.594	Q	4C04.81	st193a
2347-026	23 47 51.51	-02 41 24.4	-61	5.46	0.89	32.0	< 2	U	1.036	RG	4C-02.90	bol68

¹ The identifications are: Q = Quasar, RG = Radio Galaxy, BLRG = Broad Line Radio Galaxy, Sy2 = Seyfert 2, SB = Starburst Galaxy. Note that whilst all galaxies designated as BLRG's do show broad lines, some broad line radio galaxies may still be placed within the more general RG classification as their spectral data are not of sufficient quality to detect broad lines.

² References are given to: (a) the original optical identification or first published finding chart; (b) the first published spectroscopic redshift; (c) a high quality radio map, or, where none exist, the best radio data available in the literature. The reference labels correspond to the first three letters of the first author's name and the last two digits of the publication year, with postscripts of a,b etc for distinction where necessary; they are indicated in the reference list at the end of the manuscript. The only exception to this is the reference 'brl', which refers to the current paper.

- Allington-Smith J. R., Peacock J. A., Dunlop J. S., 1991, MNRAS, 253, 287 [all91]
- Antonucci R., 1985, ApJ Supp., 59, 499 [ant85]
- Antonucci R., 1993, ARA&A, 31, 473
- Baker J. C., Hunstead R. W., Brinkmann W., 1995, MNRAS, 277, 553 [bak95]
- Barthel P. D., 1989, ApJ, 336, 606
- Barthel P. D., Miley G. K., Schilizzi R. T., Lonsdale C. J., 1988, A&A Supp., 73, 515 [bar88]
- Baum S. A., Heckman T. M., Bridle A., van Breugel W. J. M., Miley G. K., 1988, ApJ Supp., 68, 643 [bau88]
- Bennett A. S., 1962, MemRAS, 68, 163
- Black A. R. S., Baum S. A., Leahy J. P., Perley R. A., Riley J. M., Scheuer P. A. G., 1992, MNRAS, 256, 186 [bla92]
- Bogers W. J., Hes R., Barthel P. D., Zensus J. A., 1994, A&A Supp., 105, 91 [bog94]
- Bolton J. G., Clarke M. E., Ekers R. D., 1965, Aust. J. Phys., 18, 627 [bol65]
- Bolton J. G., Ekers J., 1966a, Aust. J. Phys., 19, 471 [bol66a]
- Bolton J. G., Ekers J., 1966b, Aust. J. Phys., 19, 559 [bol66b]
- Bolton J. G., Ekers J., 1966c, Aust. J. Phys., 19, 713 [bol66c]
- Bolton J. G., Ekers J., 1966d, Aust. J. Phys., 19, 275 [bol66f]
- Bolton J. G., Kinman T. D., 1966, ApJ, 145, 951 [bol66e]
- Bolton J. G., Shimmmins A. J., Ekers J., Kinman T. D., Lamla E., Wirtanen C. A., 1966, ApJ, 144, 1229 [bol66d]
- Bolton J. G., Shimmmins A. J., Merkelijn J. K., 1968, Aust. J. Phys., 21, 81 [bol68]
- Brandie G. W., Bridle A. H., 1974, AJ, 79, 903 [bra74]
- Burbidge E. M., 1965, ApJ, 142, 1674 [bur65b]
- Burbidge E. M., 1967a, ApJ, 149, L51 [bur67]
- Burbidge E. M., 1967b, ApJ, 154, L109 [bur68]
- Burbidge E. M., Burbidge G. R., Prendergast K. H., 1962, ApJ, 136, 339 [bur62]
- Burbidge E. M., Kinman T. D., 1966, ApJ, 145, 654 [bur66]
- Burbidge E. M., Rosenberg F. D., 1965, ApJ, 142, 1673 [bur65a]
- Burbidge G. R., Burbidge E. M., 1969, Nat, 222, 735 [bur69]
- Burbidge G. R., Crowne A. H., 1979, ApJ Supp., 40, 583 [bur79]
- Cimatti A., Dey A., van Breugel W., Antonucci R., Spinrad H., 1996, ApJ, 465, 145
- Clarke M. E., Bolton J. G., Shimmmins A. J., 1966, Aust. J. Phys., 19, 375 [cla66]
- Cohen M. H., Vermeulen R. C., Ogle P. M., Tran H. D., Goodrich R. W., 1997, ApJ, 484, 193 [coh97]
- Condon J. J., Cotton W. D., Greisen E. W., Yin Q. F., Perley R. A., Taylor G. B., Broderick J. J., 1998, AJ, 115, 1693 [con98]
- Dahari O., 1985, ApJ Supp., 57, 643 [dah85]
- Danziger I. J., Goss W. M., 1983, MNRAS, 202, 703 [dan83]
- Davis R. J., Unwin S. C., Muxlow T. W. B., 1991, Nat, 354, 374 [dav91]
- Dey A., van Breugel W. J. M., Vacca W. D., Antonucci R., 1997, ApJ, 490, 698
- di Serego Alighieri S., Danziger I. J., Morganti R., Tadhunter C. N., 1994, MNRAS, 269, 998 [dis94]
- Dickinson M., 1997, in Tanvir N. R., Aragón-Salamanca A., Wall J. V., eds, HST and the high redshift Universe. Singapore: World Scientific, p. 207
- Djorgovski S., Spinrad H., McCarthy P., Dickinson M., van Breugel W. J. M., Strom R. G., 1988, AJ, 96, 836 [djo88]
- Downes A. J. B., Peacock J. A., Savage A., Carrie D. R., 1986, MNRAS, 218, 31 [dow86]
- Drinkwater M. J., Webster R. L., Francis P. J., Condon J. J., Ellison S. L., Jauncey D. J., Lovell J., Peterson B. A., Savage A., 1997, MNRAS, 284, 85 [dri97]
- Dunlop J. S., Peacock J. A., Savage A., Lilly S. J., Heasley J. N., Simon A. J. B., 1989, MNRAS, 238, 1171 [dun89]
- Eales S. A., 1985, MNRAS, 213, 899
- Eales S. A., Rawlings S., Law-Green D., Cotter G., Lacy M., 1997, MNRAS, 291, 593
- Evans D. S., 1957, Cape Atlas of Southern Galaxies [eva57]
- Fanaroff B. L., Riley J. M., 1974, MNRAS, 167, 31P
- Fejes L., Porcas R. W., Akujor C. E., 1992, A&A, 257, 459 [fej92]
- Formalont E. B., 1971, AJ, 76, 513 [for71]
- Fugmann W., Meisenheimer K., Röser H.-J., 1988, A&A Supp., 75, 173 [fug88]
- Gallimore J. F., Baum S. A., O'Dea C. P., Pedlar A., 1996, ApJ, 458, 136 [gal96]
- Giraud E., 1990, A&A, 234, L20 [gir90]
- Gopal-Krishna, Kulkarni V. K., Wiita P. J., 1996, ApJ, 463, L1
- Greenstein J. L., 1962, ApJ, 135, 679 [gre62]
- Hammer F., Le Fèvre O., 1990, ApJ, 357, 38 [ham90]
- Harvanek M., Hardcastle M. J., 1998, ApJ Supp., 119, 25 [hav98]
- Hazard C., 1965, in Robinson I., Schild A., Schucking E. L., eds, Quasi-stellar sources and gravitational collapse. Chicago: University of Chicago Press, p. 135 [haz65]
- Hazard C., 1972, ApJ, 11, L139 [haz72]
- Hazard C., Mackay M. B., Nicholson W., 1964, Nat, 202, 227 [haz64]
- Hazard C., Mackay M. B., Shimmins A. J., 1963, Nat, 197, 1037 [haz63]
- Heckman T. M., O'Dea C. P., Baum S. A., Laurikainen E., 1994, ApJ, 428, 65 [hec94]
- Hes R., Barthel P. D., Fosbury R. A. E., 1996, A&A, 313, 423 [hes96]
- Hewitt A., Burbidge G., 1991, ApJ Supp., 75, 297 [hew91]
- Hewitt A., Burbidge G., 1993, ApJ Supp., 87, 451 [hew93]
- Humason M. L., Mayall N. U., Sandage A. R., 1956, AJ, 61, 97 [hum56]
- Hunstead R. W., Murdock H. S., Shobbrook R. R., 1978, MNRAS, 185, 149 [hun78]
- Hutchings J. B., Dewey A., Chaytor D., Ryneveld S., Gower A. C., Ellingson E., 1998, PASP, 110, 111 [hut98]
- Jauncey D. L., Savage A., Morabito D. D., Preston R. A., 1989, AJ, 98, 54 [jau89]
- Junkkarinen V. T., 1984, PASP, 96, 539 [jun84]
- Kapahi V. K., Athreya R. M., Subrahmanya C. R., Baker J. C., Hunstead R. W., McCarthy P. J., van Breugel W., 1998a, ApJ Supp., 118, 327 [kap98b]
- Kapahi V. K., Athreya R. M., van Breugel W., McCarthy P. J., Subrahmanya C. R., 1998b, ApJ Supp., 118, 275 [kap98a]
- Kellermann K. I., Vermeulen R. C., Zensus J. A., Cohen M. H., 1998, AJ, 115, 1295 [kel98]
- Kinman T. D., 1966, ApJ, 144, 1232 [kin66]
- Kinman T. D., Bolton J., Clarke R., Sandage A., 1967, ApJ, 147, 848 [kin67b]
- Kinman T. D., Burbidge E. M., 1967, ApJ, 148, L59 [kin67a]
- Kristian J., Sandage A. R., 1970, ApJ, 162, 391 [kri70]
- Kristian J., Sandage A. R., Katem B., 1974, ApJ, 191, 43 [kri74]
- Laing R. A., Jenkins C. R., Wall J. V., Unger S. W., 1994, in Bicknell G. V., Dopita M. A., Quinn P. J., eds, The first Stromlo symposium: Physics of active galaxies. Cambridge University Press, Cambridge, p. 201
- Laing R. A., Riley J. M., Longair M. S., 1983, MNRAS, 204, 151
- Large M. I., Mills B. Y., Little A. G., Crawford D. F., Sutton J. M., 1981, MNRAS, 194, 693
- Law-Green J. D. B., Leahy J. P., Alexander P., Allington-Smith J. R., van Breugel W. J. M., Eales S. A., Rawlings S. G., Spinrad H., 1995, MNRAS, 274, 939 [law95]
- Lawrence A., 1991, MNRAS, 252, 586
- Lawrence C. R., Bennett C. L., Hewitt J. N., Langston G. I., Klotz S. E., Burke B. F., Turner K. C., 1986, ApJ Supp., 61, 105 [law86]
- Leahy J. P., Black A. R. S., Dennett-Thorpe J., Hardcastle M. J., Komissarov S., Perley R. A., Riley J. M., Scheuer P. A. G., 1997, MNRAS, 291, 20 [lea97]

- Lilly S. J., Longair M. S., 1984, MNRAS, 211, 833
- Lynds C. R., 1967, ApJ, 147, 837 [lyn67]
- Lynds C. R., Hill S. J., Heere K., Stockton A. N., 1966, ApJ, 144, 1244 [lyn66]
- Maddox S. J., Sutherland W. J., Efstathiou G., Loveday J., 1990, MNRAS, 243, 692
- Maltby P., Matthews T. A., Moffet A. T., 1963, ApJ, 137, 153 [mal63]
- Mantovani F., Junor W., Fanti R., Padrielli L., Browne I. W. A., Muxlow T. W. B., 1992, MNRAS, 257, 353 [man92]
- Mantovani F., Junor W., Fanti R., Padrielli L., Saikia D. J., 1997, A&A Supp., 125, 573 [man97]
- Matthews T. A., Morgan W. W., Schmidt M., 1964, ApJ, 140, 35 [mat64]
- McCarthy P. J., Kapahi V. K., van Breugel W., Persson S. E., Athreya R. M., Subrahmanya C. R., 1996, ApJ Supp., 107, 19 [mcc96]
- McCarthy P. J., van Breugel W. J. M., Spinrad H., 1989, AJ, 97, 36
- McCarthy P. J., van Breugel W. J. M., Spinrad H., Djorgovski S., 1987, ApJ, 321, L29
- Merkelijk J. K., 1969, Aust. J. Phys., 22, 237 [mer69]
- Miley G. K., 1978, A&A Supp., 34, 129 [mil78]
- Mills B. Y., 1955, Aus. J. Phys., 8, 368 [mil55]
- Morganti R., Killeen N. E. B., Tadhunter C. N., 1993, MNRAS, 263, 1023 [mor93]
- Morton D. C., Tritton K. P., 1982, MNRAS, 198, 669 [mor82]
- Nan Rendong, Schilizzi R. T., Fanti C., Fanti R., 1991, A&A, 252, 513 [nan91]
- Neff S. G., Roberts L., Hutchings J. B., 1995, ApJ Supp., 99, 349 [nef95]
- Owen F. N., O'Dea C. P., Inoue M., Eilek J. A., 1985, ApJ, 294, L85 [owe85]
- Owen F. N., White R. A., Burns J. O., 1992, ApJ Supp., 80, 501 [owe92]
- Peterson B. A., Bolton J. G., 1972, ApJ, 173, L19 [pet72]
- Peterson B. A., Bolton J. G., Shimmins A. J., 1973, Ap. Lett., 15, 109 [pet73]
- Prestage R. M., Peacock J. A., 1983, MNRAS, 204, 355 [pre83]
- Price R., Gower A. C., Hutchings J. B., Talon S., Duncan D., Ross G., 1993, ApJ Supp., 86, 365 [pri93]
- Rhee G., Marvel K., Wilson T., Roland J., Bremer M., Jackson N., Webb J., 1996, ApJ Supp., 107, 175 [rhe96]
- Riley J. M., 1989, MNRAS, 238, 1055
- Saikia D. J., Salter C. J., Muxlow T. W. B., 1987, MNRAS, 224, 911 [sai87]
- Sandage A. R., 1966, ApJ, 145, 1 [san66]
- Sandage A. R., 1967, ApJ, 150, L145 [san67]
- Sandage A. R., 1972, ApJ, 178, 25 [san72]
- Sandage A. R., Veron P., Wyndham J. D., 1965, ApJ, 142, 1307 [san65a]
- Sandage A. R., Wyndham J. D., 1965, ApJ, 141, 328 [san65b]
- Savage A., Bolton J. G., Wall J. V., 1982, MNRAS, 200, 1135 [sav82]
- Savage A., Wall J. V., 1976, Aust. J. Phys. Ap. Supp., N.39, 39 [sav76]
- Schmidt M., 1963, Nat, 197, 1040 [sch63]
- Schmidt M., 1965, ApJ, 141, 1 [sch65]
- Schmidt M., 1966, ApJ, 144, 443 [sch66]
- Searle L., Bolton J. G., 1968, ApJ, 154, L101 [sea68]
- Shen Z.-Q., Wan T.-S., Moran J. M., Jauncey D. L., Reynolds J. E., Tzioumis A. K., Gough R. G., Ferris R. H., Sinclair M. W., Jiang D.-R., Hong X.-Y., Liang S.-G., Costa M. E., Tingay S. J., McCulloch P. M., Lovell J. E. J., King E. A., Nicolson G. D., Murphy D. W., Meier D. L., van Ommen T. D., Edwards P. G., White G. L., 1997, AJ, 114, 1999 [she97]
- Singal A. K., 1993, MNRAS, 262, L27
- Smith H. E., Burbidge E. M., Spinrad H., 1976a, ApJ, 210, 627 [smi76b]
- Smith H. E., Spinrad H., 1980a, PASP, 92, 553 [smi80a]
- Smith H. E., Spinrad H., 1980b, ApJ, 236, 419 [smi80b]
- Smith H. E., Spinrad H., Hunstead R., 1976b, ApJ, 206, 345 [smi76a]
- Smith H. E., Spinrad H., Smith E. G., 1976c, PASP, 88, 621 [smi76c]
- Spinrad H., Djorgovski S., 1984, ApJ, 285, L49 [spi84]
- Spinrad H., Djorgovski S., Marr J., Aguilar L. A., 1985a, PASP, 97, 932 [spi85a]
- Spinrad H., Filippenko A., Wyckoff S., Stocke J., Wagner M., Lawrie D., 1985b, ApJ, 299, L7 [spi85b]
- Spinrad H., Kron R. G., Hunstead R., 1979, ApJ Supp., 41, 701 [spi79]
- Spinrad H., Liebert J., Smith H. E., Hunstead R., 1976, ApJ, 206, L79 [spi76]
- Spinrad H., Smith H. E., Hunstead R., Ryle M., 1975, ApJ, 198, 7 [spi75]
- Stickel M., Kühr H., 1993, A&A Supp., 100, 395 [sti93b]
- Stickel M., Kühr H., Fried J. W., 1993, A&A Supp., 97, 483 [sti93a]
- Swain M. R., Bridle A. H., Baum S. A., 1996, in Hardee P. E., Bridle A. H., Zensus J. A., eds, Energy transport in radio galaxies and quasars. [swa96] ASP Conf. Ser. 100, San Francisco, p. 299
- Swarup G., Saikia D. J., Beltrametti M., Sinha R. P., Salter C. J., 1986, MNRAS, 220, 1 [swa86]
- Tadhunter C. N., Morganti R., di Serego Alighieri S., Fosbury R. A. E., 1993, MNRAS, 263, 999 [tad93]
- Veron-Cetty M.-P., Veron P., 1996, ESO Scientific Report, 17, 1 [ver96]
- Vorontsov-Vel'yaminov B., 1959, Atlas and Catalogue of Interacting Galaxies, Part 1. Moscow State Univ., Moscow [vor59]
- Walker R. C., Benson J. M., Unwin S. C., 1987, ApJ, 316, 546 [wal87]
- Wall J. V., Peacock J. A., 1985, MNRAS, 216, 173
- Walter H. G., West R. M., 1980, A&A, 86, 1 [wal80]
- Weedman D. W., 1976, ApJ, 208, 30 [wee76]
- Willott C. J., Rawlings S., Blundell K. M., Lacy M., 1998, MNRAS, 300, 625
- Willott C. J., Rawlings S., Jarvis M., 1999, MNRAS: in press
- Wills B. J., Wills D., 1979, ApJ Supp., 41, 689 [wil79]
- Wills D., Wills B. J., 1981, Nat, 289, 384 [wil81]
- Wright A., Otrupcek R., 1990, Parkes Catalogue. Australia Telescope National Facility [wri90]
- Wright A. E., Ables J. G., Allen D. A., 1983, MNRAS, 205, 793 [wri83]
- Wroblewski H., Costa E., Torres C., 1981, A&A, 93, 245 [wro81]
- Wyndham J. D., 1965, AJ, 70, 384 [wyn65]
- Wyndham J. D., 1966, ApJ, 144, 459 [wyn66]